HHS Public Access

Author manuscript

Neuron. Author manuscript; available in PMC 2022 January 06.

Published in final edited form as:

Neuron. 2021 January 06; 109(1): 123–134.e4. doi:10.1016/j.neuron.2020.09.037.

Relocation of an extrasynaptic $GABA_A$ receptor to inhibitory synapses freezes excitatory synaptic strength and preserves memory

Christopher M. Davenport[1,3], **Rajit Rajappa**[1,3], **Ljudmila Katchan**[1], **Charlotte R. Taylor**[1], **Ming-Chi Tsai**[1], **Caleb M. Smith**[1], **Johannes de Jong**[1], **Don B. Arnold**[2], **Stephan Lammel**[1], **Richard H. Kramer**[1,4]

[1:]Department of Molecular and Cell Biology, University of California, Berkeley, Berkeley CA, 94720, USA

[2:]Department of Biology, Section of Molecular and Computational Biology, University of Southern California, Los Angeles, Los Angeles CA, 90089, USA

[3:]These authors contributed equally

Summary

The excitatory synapse between hippocampal CA3 and CA1 pyramidal neurons exhibits long-term potentiation (LTP), a positive feedback process implicated in learning and memory, in which postsynaptic depolarization strengthens synapses, promoting further depolarization. Without mechanisms for interrupting positive feedback, excitatory synapses could strengthen inexorably, corrupting memory storage. Here we reveal a hidden form of inhibitory synaptic plasticity that prevents accumulation of excitatory LTP. We developed a knock-in mouse that allows optical control of endogenous α5-subunit-containing $GABA_A$ receptors (α5-GABARs). Induction of excitatory LTP relocates α5-GABARs, which are ordinarily extrasynaptic, to inhibitory synapses, quashing further NMDA receptor activation necessary for inducing more excitatory LTP. Blockade of α5-GABARs accelerates reversal learning, a behavioral test for cognitive flexibility dependent on repeated LTP. Hence inhibitory synaptic plasticity occurs in parallel with excitatory synaptic plasticity, with the ensuing interruption of the positive feedback cycle of LTP serving as a possible critical early step in preserving memory.

Graphical Abstract

[4]Lead contact and corresponding author: rhkramer@berkeley.edu.

Author Contributions

Conceptualization, C.M.D., R.R., L.K., and R.H.K.; Investigation: C.M.D., R.R., L.K., C.R.T., M.C.T., C.M.S., J.d.J.; Resources, D.B.A., and S.L.; Writing, C.M.D., R.R., C.R.T., and R.H.K.; Funding Acquisition, R.H.K.; Supervision, R.H.K.

Declaration of Interests

The authors declare no competing interests

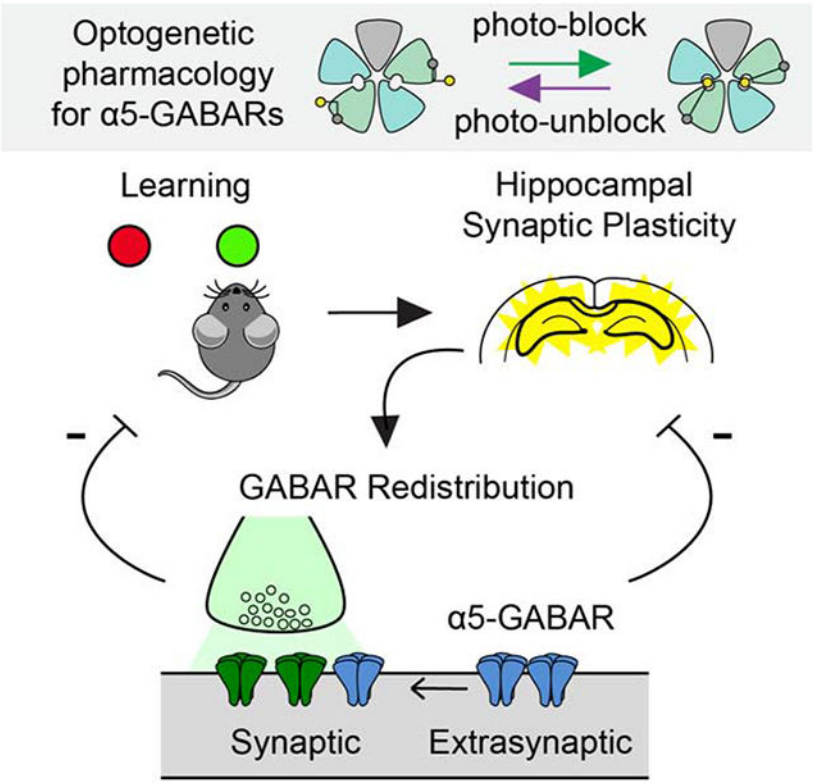

eTOC Blurb

Long-term potentiation (LTP) of excitatory synaptic transmission strengthens neural circuit connections during learning. Davenport, Rajappa, et al. show with optogenetic pharmacology that a specific receptor for the neurotransmitter GABA redistributes to inhibitory synapses, prolonging synaptic inhibition. This breaks the positive-feedback of excitatory LTP to freeze synaptic strength and preserve memory.

Keywords

GABA receptors; synaptic plasticity; metaplasticity; memory; optogenetic pharmacology

Introduction

Long-term potentiation (LTP) and long-term depression (LTD) of excitatory glutamatergic synaptic transmission are elementary mechanisms for establishing memories in the mammalian brain (Takeuchi et al., 2014). Understanding how LTP and LTD are induced and maintained has required pharmacological blockade of inhibitory γ-aminobutyric acid (GABA)-ergic synapses, which otherwise would obscure excitatory synaptic events (Wigstrom and Gustafsson, 1983). However, inhibitory neurotransmission itself exhibits plasticity, owing to presynaptic changes in GABA release or postsynaptic changes in GABA receptiveness (Castillo et al., 2011). Changing the strength of inhibition can directly alter the firing output of a neuron, but inhibitory plasticity can also affect activity-dependent

excitatory plasticity, an interplay known as metaplasticity (Wang et al., 2014; Zorumski and Izumi, 2012).

Rapid responses to GABA are mediated by $GABA_A$ receptors, pentameric proteins composed of alpha, beta, and tertiary subunits (Sieghart et al., 1999). Receptors containing the α5 subunit (α5-GABARs) are strikingly enriched in the hippocampus (Fritschy and Mohler, 1995), hinting at their importance for learning and memory and raising the possibility of α5-GABARs as a drug target for cognitive enhancement (Dawson et al., 2006). Supporting this idea, selective pharmacological modulation (Dawson et al., 2006) or genetic suppression or removal of α5-GABARs (Collinson et al., 2002; Crestani et al., 2002) improves certain forms of learning in mice.

α5-GABARs were originally characterized as extrasynaptic, mediating tonic inhibition, whereas α1-GABARs are synaptic, mediating rapid inhibition (Glykys and Mody, 2006; Serwanski et al., 2006). In cultured hippocampal neurons, α5-GABARs were found exclusively in extrasynaptic puncta, colocalized with the cytoskeletal-associated protein radixin (Loebrich et al., 2006). However, recent studies utilizing a selective pharmacological modulator implicate α5-GABARs in synaptic inhibition (Schulz et al., 2018). This contradiction might be explained by the finding that chemical depolarization leads to α5-GABARs dissociating from radixin and migrating to puncta containing gephyrin (Hausrat et al., 2015), a scaffolding protein at inhibitory synapses (Moss and Smart, 2001). This suggests that dynamic redistribution of α5-GABARs is functionally important, but understanding the role of α5-GABARs in metaplasticity, learning, and memory requires analysis in the intact neural circuit.

The best known example of excitatory LTP takes place at the synapse between Schaffer collaterals of CA3 and CA1 pyramidal neurons in the hippocampus, requiring multiple types of glutamate receptors (Nicoll, 2017). AMPARs mediate rapid excitatory transmission whereas N-methyl D-aspartate receptors (NMDARs) induce plasticity by triggering the insertion of new postsynaptic AMPARs. The discovery of antagonists specific for AMPAR and NMDARs was essential for elucidating how LTP is induced and maintained (Davies and Collingridge, 1989). In contrast, there are no known subtype-specific antagonists for $GABA_A$ receptors. The role of α5-GABARs has been inferred with pharmacological modulators acting on the allosteric benzodiazepine binding site (Rudolph and Möhler, 2014). The delivery of pharmacological agents is slow, particularly in intact neural tissue, impeding an understanding of how these receptors affect excitatory synaptic plasticity, learning, and memory. Gene knock-out technology can remove a specific α-subunit, but compensatory changes in the expression of other receptors or channels can confound interpretation of the resulting phenotype (Brickley et al., 2001; Kralic et al., 2002; Ponomarev et al., 2006).

To better understand the physiological role of α5-GABARs, we used a different approach that combines the specificity afforded by genetics, the reversibility afforded by pharmacology, and the temporal and spatial precision afforded by optical control. We impart light sensitivity onto specific genetically tagged GABAR α-subunits by conjugating a photoswitchable tethered ligand (PTL) onto a cysteine-mutant of the receptor. Susceptibility

to the PTL is built-in to the receptor, specified by which subunit has the mutation. A knock-in mouse with a genomic cysteine mutation allows photocontrol of the endogenous receptor, with its expression pattern pre-determined by intrinsic genetic programs.

Results

To exert photocontrol over endogenous $GABA_A$ isoforms, we generated knock-in mice with a genomically encoded cysteine mutation in a particular subunit. We previously reported a knock-in mouse with a cysteine mutation in the α1 subunit (Lin et al., 2015). Here we introduce a knock-in mouse with a cysteine mutation in the α5 subunit (α5-E125C-KI). $GABA_A$ receptors containing the mutant α5 have functional properties indistinguishable from receptors containing wild-type α5, apart from light-dependent block ("photo-block") after conjugation to the azobenzene photoswitch PAG1C (Figure 1A; Lin et al., 2015). To verify unaltered expression levels in the brain, we probed with an anti-α5 antibody and found comparable protein levels in α5-E125C-KI and wild-type (WT) mice, with hippocampus > olfactory bulb > cerebral cortex > cerebellum for both. Moreover, immunolabeling showed identical expression patterns across the hippocampus of α5-E125C-KI and WT mice (Figure S1).

In quiescent neurons, α5-GABARs contribute to tonic, not synaptic, inhibition

The α5 subunit is thought to be largely extrasynaptic, mediating tonic inhibition (Caraiscos et al., 2004). To assess the contribution of α5-GABARs to synaptic vs. tonic inhibition, we recorded from CA1 pyramidal neurons in α5-E125C-KI hippocampal slices treated with PAG1C to photosensitize the receptors. The neurons were voltage-clamped at the reversal potential for excitatory postsynaptic currents (EPSCs; 0 mV) to isolate inhibitory postsynaptic currents (IPSCs). Under these conditions, we found no photo-block of IPSCs (Figure 1B; photo-block = 1.5 ± 1.3 %). However over-expressing the mutant α5 enabled significant photo-block (Figure 1C; 46 ± 6.9 %, t-test $p < 0.001$). Therefore while α5-GABARs can integrate into inhibitory synapses, under baseline conditions there is no synaptic contribution. In contrast, tonic GABAergic current decreased significantly when α5-GABARs were photo-blocked (Figure 1D,E; photo-block = 16 ± 2.5 %, paired t-test $p = 0.024$). As expected, the tonic current was abolished by the GABAR antagonist picrotoxin (Figure 1D). There was no photo-block without PAG1C or in WT mice lacking the α5 cysteine mutation (Figure 1E)

α5-GABARs suppress induction of LTD, but not LTP

We next asked whether α5-GABARs contribute to long-term synaptic plasticity. Schaffer collaterals of CA3 pyramidal neurons form excitatory synapses on CA1 pyramidal neurons, and also recruit GABAergic interneurons, which form inhibitory synapses onto the same CA1 neurons (Buszáki, 1984). To study the interaction between inhibition and excitation during LTP induction, we delivered theta burst stimulation (TBS) to the Schaffer collaterals to induce LTP in α5-E125C-KI hippocampal slices, and photo-controlled the receptors during TBS only. LTP was measured by monitoring the initial slope of field excitatory postsynaptic potentials (fEPSP) in the stratum radiatum (SR). Photo-blocking α5-GABARs

had no effect on LTP induced by a single TBS (Figure 2A, B; LTP_{540}= 1.39 ± 0.1, n = 6; LTP_{390}= 1.46 ± 0.1, t-test p = 0.67), consistent with their absence from inhibitory synapses.

Induction of excitatory LTP in CA1 neurons relies on activation of NMDARs localized to excitatory synapses. In contrast, excitatory LTD involves both synaptic and extrasynaptic NMDARs (Papouin et al., 2012; Rusakov et al., 2004). Like for LTP, GABARs were blocked in most prior studies of LTD. With inhibition intact, we found that low frequency stimulation (1 Hz, 900 stimuli) elicited neither LTP or LTD, regardless of α5-GABAR photo-block (Figure 2C, D). However, a higher stimulation frequency (10 Hz, 100 stimuli) elicited LTD but only when α5-GABARs were photo-blocked (Figure 2E,F; t-test p = 0.015). These findings suggest that under quiescent conditions, α5-GABARs can suppress excitatory plasticity mediated by extrasynaptic NMDARs (i.e., LTD), but not plasticity mediated by synaptic NMDARs (i.e., LTP).

α5-GABARs prevent cumulative LTP, induced by repeated high frequency stimulation

A different picture emerged when we attempted to elicit multiple rounds of LTP. We applied four TBS episodes, 20 min apart. With α5-GABARs unblocked during the TBS, fEPSP slope was 1.6-fold greater than baseline after the first round of stimuli, 1.9-fold greater after the second round, and then saturated, remaining at ~1.9-fold greater after the 3rd and 4th rounds (Fig 3A, B; LTP_{4th}/LTP_{2nd} = 1.07 ± 0.13, paired t-test p = 0.60). When α5-GABARs were photo-blocked during the TBS, LTP increased for the first and second rounds of stimulation, but continued to grow over the 3rd and 4th rounds (Figure 3B, I; LTP_{4th}/LTP_{2nd} = 1.29 ± 0.11, rank sum test p = 0.03). Hence photo-block of α5-GABARs prevented the apparent saturation of LTP. Studies on α5 knockout mice (α5-KO) led to the same conclusion. In WT mice, LTP saturated within two rounds of TBS, but in α5-KO mice, LTP continued to grow over all four rounds of stimulation (Figure 3C, D; WT LTP_{4th}/LTP_{2nd}=1.08 ± 0.05, paired t-test p = 0.1; KO LTP_{4th}/LTP_{2nd}= 1.25 ± 0.07, paired t-test p = 0.03). These results were further supported by experiments using an inverse agonist to the α5-GABAR, TB-21007 (Figure 3E, F). In the presence of TB-21007 LTP exhibited less saturation compared to control slices (control LTP_{4th}/LTP_{2nd} = 1.13 ± 0.13, n = 6 slices, TB-21007 LTP_{4th}/LTP_{2nd}= 1.54 ± 0.11, t-test p = 0.04). The lack of apparent saturation of LTP in α5-KO mice and after inhibiting α5-GABAR further supports a critical role of these receptors in restraining runaway LTP. We cannot rule out possible off-target effects of TB-21007, in contrast to our photo-block strategy, which is specific for α5-GABARs.

For comparison, we examined the effect of photo-blocking α1-GABARs on accumulation of LTP. We used PAG1C to photosensitize α1-GABARs in hippocampal slices from mutant α1 knock-in mice (α1-T125C; Lin et al., 2015). Photo-block of α1-GABARs had no effect on the accumulation of LTP (Figure 3G, H; blocked LTP_{4th}/LTP_{2nd}= 1.08 ± 0.12; unblocked LTP_{4th}/LTP_{2n}=0.99 ± 0.15, paired t-test p = 0.47), even though α1-GABAR is a major contributor to inhibitory synaptic currents (Lin et al., 2015). Hence α5-GABARs are uniquely able to suppress LTP, but in an activity-dependent manner. Taken together, these results suggest that under physiological conditions, the dominant mechanism capping the growth of LTP is not saturation of a biochemical step in LTP induction, but rather the rise of an opposing inhibitory process that actively suppresses potentiation. We found that field

potential responses to test stimuli were unaffected by photo-block of α5-GABARs both before and after LTP (Figure S2), indicating that while α5-GABARs acquire the ability to suppress induction of LTP, they have no effect on the maintenance of LTP that has already occurred.

Stimulation drives α5-GABARs into inhibitory synapses, suppressing excitatory synaptic responses mediated by NMDARs

Imaging studies of cultured dissociated neurons show that a chemical treatment intended to mimic LTP causes disappearance of α5-GABARs from puncta labeling for the extrasynaptic cytoskeletal-associated protein radixin and appearance at puncta labeling for gephyrin (Hausrat et al., 2015), often associated with inhibitory synapses (Tretter et al., 2012). To test whether α5-GABARs integrate into inhibitory synapses during LTP in the hippocampal circuit, we electrically stimulated SC inputs and measured photo-block of polysynaptic IPSCs in CA1 pyramidal neurons in brain slices from α5C-E125C-KI mice. The ability to induce LTP tends to diminish during whole-cell recording, owing to wash-out of critical cytoplasmic components (Malinow and Tsien, 1990). Therefore we used a cell sampling strategy, assaying one group of neurons patched before applying TBS, and then a different group of neurons patched 30 min after TBS. The contribution of α5-GABARs to IPSCs evoked by a single stimulus was small and not significantly different in neurons sampled before or after TBS (Figure 4A, B; photo-block before TBS = 5.1 ± 1.6 %, photo-block after TBS = 10.2 ± 4.7%, t-test p = 0.33). However, when IPSCs were evoked by a brief train of stimuli (5 pulses at 100 Hz) α5-GABARs made a significant contribution, but only in cells sampled after TBS (Figure 4C, D; photo-block before TBS = −2.4 ± 0.8 %; post TBS = 15 ± 4.2 %, t-test p = 0.017). The participation of α5-GABARs in responses to trains of stimuli, but not single stimuli, might be due to receptors being added perisynaptically, where GABA accumulates only after multiple presynaptic action potentials (Weir et al., 2017).

Our results suggest that initially, α5-GABARs are extrasynaptic, but stimulation of excitatory inputs alters the balance, increasing the synaptic contribution. The ratio of extrasynaptic to synaptic receptors differs between neuronal cell types. Layer 2 pyramidal neurons in visual cortex had significant resting synaptic contribution of α5-GABARs (Figure S3 A, B). Newborn granule cells in the dentate gyrus of the hippocampus (Toda and Gage, 2018), also had significant resting synaptic contribution (Figure S4 F-H). However, this declined as the granule cells matured and integrated into the hippocampal circuit, paralleled by increasing α5-GABAR contribution to tonic inhibition (Figure S4 A-E). In mature granule cells, induction of LTP reduced the tonic contribution and increased the synaptic contribution (Figure S4 A-E). Together, these results indicate that developmental and activity-dependent events shift the localization of the receptors between extrasynaptic and synaptic sites, thereby altering the functional impact of α5-GABARs.

Synaptic inhibition of pyramidal neurons is mediated by several classes of GABAergic interneurons (Pelkey et al., 2017). These include Somatostatin (SOM) cells, which preferentially contact distal dendrites, and Parvalbumin (PV) cells, which preferentially contact proximal dendrites or somata (Bezaire and Soltesz, 2013). Since α5-GABARs affect cumulative LTP, which occurs primarily in dendrites, relocation might occur selectively at

SOM synapses. To test this, we generated α5-E125C-KI mice in which either SOM or PV cells express a red-shifted version of channelrhodopsin (ReaChR). ReaChR is activated by wavelengths of light that do not isomerize the azobenzene moiety of PAG1C (Mourot et al., 2011), allowing presynaptic interneuron firing to be controlled independent from postsynaptic α5-GABAR activity. Initially, optogentically triggered IPSCs from SOM or PV cells were unaffected by photo-blocking α5-GABARs (Figure S5 A-D). However, after TBS, SOM-evoked IPSCs but not PV-evoked IPSCs were reduced by photo-blocking, consistent with redistribution of α5-GABAR to SOM synapses (Figure S5 A-D). The selective change in SOM synapses is consistent with a type of NMDAR-mediated inhibitory LTP that is selective for SOM cells in cortex (Chiu et al., 2018).

Stimulation of Schaffer collaterals can induce not only monosynaptic plasticity, but also polysynaptic effects, for example LTP at excitatory inputs onto inhibitory interneurons that in turn synapse on CA1 neurons (Pelletier and Lacaille, 2008). To confirm that the synaptic redistribution of α5-GABAR is specific to the monosynaptic connection, we included the NMDAR antagonist MK-801 (1 mM) in the patch pipette. MK-801 is membrane-impermeant and can block NMDARs from the intracellular side (Berretta and Jones, 1996). Additionally, we voltage-clamped the membrane potential to −70 mV to suppress LTP induction (Malinow and Tsien, 1990) and waited >10 minutes before TBS, to promote wash-out of constituents necessary for LTP induction. Under these conditions, TBS failed to increase the synaptic contribution of α5-GABARs (Figure 4C, D; photo-block = −0.8 ± 1.5 %, t-test p = 0.43). This confirms that the increased α5-GABAR contribution requires LTP in the postsynaptic CA1 cell and indicates that the redistribution of α5-GABARs requires a NMDAR-mediated signal, likely via an increase in cytoplasmic Ca^{2+}.

One way that α5-GABARs might prevent induction of LTP is by suppressing the depolarization necessary for relieving Mg^{2+} block of NMDARs (Hayama et al., 2013; Mayer et al., 1984). To measure the impact of α5-GABARs on NMDAR activation we recorded the synaptic voltage response of separate CA1 neurons in the same slice before or after TBS. In neurons sampled before TBS, a stimulus train caused a brief mixed EPSP/IPSP, and triggered 2-3 spikes (Figure 4E). The response was unaffected by photo-block (Figure 4E, F; photo-block of response area = −14 ± 6.0 %), consistent with the initial absence of α5-GABAR from synapses. However, in neurons sampled after TBS, the train triggered a regenerative response characterized by sustained action potential firing (6-10 spikes) and a prolonged plateau of depolarization, but only when α5-GABARs were photo-blocked (Figure 4E, F; photo-block = 35 ± 7.9 %, t-test p = 0.02). The regenerative response was eliminated by the NMDAR blocker APV (50 μM; Figure 4E, F; photo-block = −12 ± 11 %, t-test p = 0.34). Hence the activity-dependent migration of α5-GABARs to synapses is correlated with attenuation of NMDAR-dependent regenerative responses and suppression of cumulative LTP.

NMDARs have slower kinetics than other ionotropic glutamate receptors and therefore generate slower and longer-lasting synaptic responses (Jahr, 1994). Studies utilizing pharmacological or genetic manipulation suggest that α5-GABARs also have slower kinetics than classical synaptic types of GABARs (α1, α2, or α3) (Picton and Fisher, 2007; Zarnowska et al., 2009). To directly measure the kinetics of α5-GABARs at synapses we

over-expressed α5-E125C in cortical neurons. For comparison, we over-expressed α1-T125C. Photo-block experiments showed that the light-sensitive component of a single IPSC was 2-4-fold slower in both rise and decay times when α5 was overexpressed compared to when α1 was overexpressed (Figure S6). The slow kinetics may make α5-GABARs particularly effective in suppressing NMDAR responses, especially when high frequency presynaptic stimulation leads to the lingering presence of both GABA and glutamate.

Our results imply that strengthening of synaptic inhibition, induced by prior excitatory LTP, suppresses induction of additional excitatory LTP. To directly verify this in a continuous recording from an individual cell, we recorded the membrane potential of a CA1 neuron and delivered multiple rounds of TBS to input axons (Figure S7). The first TBS induced significant LTP of responses to test stimuli (Figure S7 A-D; 1.67 ± 0.11, paired t-test vs baseline $p = 0.0006$) while the second TBS produced no additional LTP (Figure S7 A-D; 1.68 ± 0.23, $p = 0.95$ vs 1st, paired t-test). Next, we analyzed the complex voltage response during and immediately after a TBS, comprised of overlapping EPSPs and IPSPs. The long latency portion of the TBS-induced response (>10 msec after each train), consisted of a net depolarization for the first round of TBS (Fig S7 E, F; 1st TBS area = 22.9 ± 5.9), but became increasingly hyperpolarizing for the second and third rounds (3rd TBS area = −10.3 ± 5.6 $p = 0.012$ vs 1st, paired t-test). The short latency responses following each stimulus were depolarizing in all cases (Figure S7 G, H). These results suggest that TBS strengthens a slow inhibitory component, presumably mediated by α5-GABARs, which suppresses a late excitatory component, presumably mediated by NMDARs.

Redistribution of α5-GABARs to inhibitory synapses requires radixin dephosphorylation

Single molecule imaging studies in cultured hippocampal neurons suggest that radixin establishes a cache of extrasynaptic α5-GABARs that can be recruited into synaptic service in an activity-dependent manner (Hausrat et al., 2015). Binding of α5-GABARs requires phosphorylation of a specific threonine (T564) in radixin (Matsui et al., 1998; Loebrich et al., 2006). To test the role of radixin in activity-dependent receptor redistribution, we replaced T564 with a phosphorylation incompetent alanine (radixin-T564A) to preclude α5-GABAR binding, or with a phosphorylation-mimicking aspartate (radixin-T564D) to promote α5-GABAR binding (Figure 5A). We injected AAV encoding either of these mutants into the hippocampus of α5-E125C-KI mice, and subsequently measured the effect of α5-GABAR photo-block on evoked IPSCs. At rest, CA1 neurons transduced by the radixin-T564A virus showed a light-dependent change in IPSCs, indicating a significant synaptic contribution of α5-GABARs, even without TBS (Figure 5B, C photo-block WT = 4 ± 1.6 %; T564A = 13.4 ± 2.3 %, $n = 9$ cells; t-test $p = 0.009$). This suggests that disrupting α5-GABAR binding to radixin frees the receptors to incorporate into inhibitory synapses. The relaxation kinetics of the light-sensitive component of the IPSC was slower than that of the total IPSC ($\tau = 67.18$ ms vs. $\tau = 32.99$ ms, Figure 5D), consistent with α5-GABARs having slower kinetics than typical synaptic GABAR isoforms. In contrast, in CA1 neurons transduced by the phosphomimetic radixin-T564D, photo-block had no effect on IPSCs, even after applying TBS (Figure 5E, F photo-block WT before TBS = 3.56 ± 1.5 %; WT after TBS = 15.6 ± 1.4 %; T564A after TBS = −6 ± 5.8 %; One way ANOVA $p < 0.0001$). This suggests that stabilizing the binding of radixin to α5-GABARs prevents the

redistribution of the receptors to inhibitory synapses. Together, these results support the hypothesis that excitatory synaptic stimulation drives α5-GABARs from extrasynaptic to inhibitory synaptic sites, changing the kinetic properties of inhibitory synaptic transmission.

The gephyrin scaffold at inhibitory synapses is necessary for α5-GABAR suppression of cumulative LTP

We next tested whether inhibitory synapses are necessary for suppressing the accumulation of LTP. We employed a genetically-encoded intrabody, GFE3, that targets gephryin with E3 ligase, promoting ubiquitination and lysosomal degradation (Gross et al., 2016). By ablating gephryin, GFE3 disrupts inhibitory synapses and disperses GABARs in the surface membrane. If the migration of α5-GABARs to inhibitory synapses is necessary for suppressing cumulative LTP, ablating gephyrin should enable LTP to continue to grow with repeated rounds of stimulation. We quantified the functional disruption of inhibitory synapses by measuring the relative amplitude of evoked EPSPs at rest where glutamatergic responses are depolarizing and IPSPs at − 55 mV, where GABAergic responses are hyperpolarizing (E/I ratio; Figure 6A, B). In CA1 neurons from mice injected with an AAV vector encoding GFE3, the E/I ratio was high and very variable (mean = 1.90; S.D. = 0.85, range = 0.69 to 3.68; rank sum test vs. control = 0.03) consistent with different degrees of inhibitory synapse disruption, while in uninjected controls, the E/I ratio was consistently low (mean = 0.90; S.D. = 0.19, range = 0.69 to 1.2).

We applied four rounds of TBS and patched a sampling of neurons either before the first or the fourth round to compare induction of LTP in naive neurons with induction in neurons whose synapses should have already been potentiated (Figure 6C). Without the GFE3 virus, EPSPs were potentiated much more by the first TBS (1.87 ± 0.11, n = 5), than by the fourth (1.37 ± 0.07; p = 0.008), such that the ratio was 0.74 ± 0.03 (Figure 6D, E), consistent with suppression of cumulative LTP. With the GFE3 virus, EPSPs were potentiated equally by both rounds of TBS (ratio = 1.08 ± 0.22; p = 0.705) (Figure 6D, E). We noted a high degree of variability in LTP induced in GFE3-expressing neurons. However, a strong correlation emerged when we accounted for the degree of disruption of inhibitory synapses. Neurons with the least inhibition (large E/I ratio) showed the highest degree of potentiation on the fourth round of stimulation, while neurons with the most inhibition (small E/I ratio) had potentiation that was similar to neurons from mice without GFE3 (Figure 6F; Pearson's r = 0.898, p = 0.001). Taken together, these results indicate that inhibitory synapses are necessary for suppression of cumulative LTP.

Reversal learning is enhanced by blocking hippocampal α5-GABARs *in vivo*

Our discovery that the α5-GABAR places a cap on cumulative LTP leads to the prediction that α5-GABAR block will promote learning that requires repeated episodes of synaptic plasticity. PAG1C effectively conjugates and blocks cysteine-substituted GABARs *in vivo* (Lin et al., 2015), but since GABARs are continually inserted and removed from the plasma membrane, the modified receptors may have a lifespan as brief as 24 hours (Saliba et al., 2007). Therefore, we sought a form of learning that could be completed within several hours of PAG1C treatment. One such task is reversal learning, which measures an animal's active suppression of a reward-related response to one stimulus and initiation of a response to a

different, previously unrewarded stimulus (Laughlin et al., 2011). To elicit reversal learning, we used an operant conditioning chamber (Figure 7A), with two nose poke holes associated either with reward (sugar pellet) or no reward. To confirm that reversal learning requires NMDAR-dependent plasticity, we injected APV bilaterally in the hippocampi of α5-E125C-KI mice to locally block NMDARs after learning, but before reversal learning. Mice receiving APV showed slow and incomplete reversal of the learned association as compared to vehicle-injected control mice (Figure 7B, C ANOVA, $F(3,17) = 3.246$, $p = 0.0479$) and trial R-5 (ANOVA, $F(3,17) = 4.611$, $p = 0.0155$), indicating that NMDAR-dependent plasticity is required for reversal learning.

We next tested the involvement of α5-GABARs in reversal learning. Injection of PAG1C into the hippocampus of α5-E125C-KI mice resulted in faster reversal learning than in α5-E125C-KI mice injected with saline or WT mice injected with PAG1C (Figure 7B, D). WT and α5-E125C-KI mice without PAG1C learned the association equally well (Figure 7B). These findings, along with our electrophysiological results, suggest that by inhibiting LTD and suppressing accumulation of LTP, α5-GABARs sustain previously learned associations, and inhibit behavioral flexibility.

Discussion

Long-term synaptic plasticity is critical for neural circuit refinement during development and information storage during learning (Bliss and Collingridge, 2019). LTP is a positive feedback process that left unchecked would saturate and lead to neural hyperactivity, impairing information storage and causing excitotoxicity or epilepsy. Therefore, the processes underlying long-term synaptic plasticity must themselves be flexible, to adjust for prior synaptic plasticity. The plasticity of plasticity is termed metaplasticity.

Metaplasticity can either promote or suppress excitatory synaptic plasticity (Abraham and Bear, 1996). For example, moderate activation of NMDARs that by itself causes no plasticity can nonetheless raise the threshold for inducing LTP (Huang et al., 1992; Zorumski and Izumi, 2012). By contrast, glutamate released onto CA1 neurons can lead to retrograde endocannabinoid signalling to presynaptic terminals of inhibitory interneurons, depressing GABA release (Chevaleyre and Castillo, 2004). The net result is to promote further LTP in the CA1 neuron. The relative strength of mechanisms that either enhance or suppress plasticity depends on many factors, including developmental stage (Dunfield and Haas, 2009), behavioral state (Vose and Stanton, 2017), and the specific temporal requirements of learning (Xu et al., 2014).

Our results reveal a previously hidden mechanism of metaplasticity. At rest (Figure 8A), inhibitory synapses onto CA1 neurons have many α1-GABARs, but few α5-GABARs. Meanwhile, excitatory synapses possess AMPARs, which carry most of the synaptic current, and NMDARs, which are largely inert owing to voltage-dependent Mg^{2+} block. High frequency stimulation of excitatory inputs (Figure 8B) depolarizes postsynaptic sites sufficient to alleviate Mg^{2+} block, allowing NMDARs to participate in excitatory synaptic current and to conduct Ca^{2+}. This leads to dephosphorylation of radixin, which frees α5-GABARs bound in extrasynaptic clusters to diffuse through the membrane and become

trapped by gephyrin at inhibitory synapses. Once α5-GABARs have incorporated into these synapses (Figure 8C), their slower inhibitory synaptic current more closely matches the kinetics of NMDARs, keeping them from becoming unblocked and thereby preventing induction of more excitatory LTP.

What is the evidence for this scenario? First, the proposed distribution of functional $GABA_A$ receptor isoforms in quiescent neurons is supported by pharmacology (Thomson et al., 2000), immunolabeling (Brunig et al., 2002; Kasugai et al., 2010), and photoswitching (Lin et al., 2015) studies, which all indicate that α1-GABARs make a major contribution to inhibitory synaptic current. For example, in photoswitching experiments, local photolysis of caged GABA on CA1 neurons with light-sensitive α1-GABARs showed hotspots of photo-block identical with sites of gephyrin labeling (Lin et al., 2015). In actuality, α1 is not alone at the synapse; α2 and α3-containing GABARs also make a major contribution, either heteromultimerized with one another or with α1 subunits (Prenosil et al., 2006; Sieghart and Sperk, 2002). In photo-block experiments using α5-E125C-KI mice we show no α5-GABAR contribution to inhibitory synaptic current, but significant contribution to tonic current. These results are consistent with previous studies implicating α5-GABAR as extrasynaptic (Caraiscos et al. 2004; Serwanski et al., 2006; Hausrat et al., 2015).

Several types of evidence support the second part of our model; that α5-GABARs redistribute to inhibitory synapses in an activity-dependent manner. Single molecule immunofluorescent tracking of α5-GABARs show that chemical depolarization mobilizes extrasynaptic receptors, allowing them to diffuse laterally and become trapped at gephyrin-labeled sites, presumably inhibitory synapses (Hausrat et al., 2015). Our photo-block results show that after high frequency synaptic stimulation, α5-GABARs begin contributing to IPSCs, specifically those originating from the SOM class of inhibitory interneurons, which preferentially contact distal dendrites of CA1 neurons (Bezaire and Soltesz, 2013). Our findings support previous biochemical and optical imaging results implicating radixin as the extrasynaptic scaffold for α5-GABARs and gephyrin as a synaptic scaffold (Hausrat et al, 2015; Brady and Jacob, 2015).

It seems likely that redistribution of α5-GABARs is a reversible process, with activity weakening radixin binding and inactivity strengthening it. The balance between extrasynaptic and synaptic localization may also be regulated developmentally, and in a cell-type selective manner. Thus, we find that even without stimulation, α5-GABARs contribute significantly to IPSCs in pyramidal neurons from the visual cortex and in newborn granule cells in the dentate gyrus, although there, the receptors shift from synaptic to extrasynaptic as the neurons mature and integrate in the hippocampal circuit. Previous findings of α5-GABARs at inhibitory synapses on CA1 neurons (Schulz et al., 2018) may reflect a higher level of baseline activity.

Our photo-block results support the third part of our model; that synaptically redistributed α5-GABARs suppress NMDAR-dependent induction of further LTP. The relocation of α5-GABARs exposes the receptors to locally high concentrations of GABA in or near the synaptic cleft. The relatively slow relaxation kinetics of α5-GABARs more closely overlap with the slow kinetics of NMDARs at excitatory synapses, and both the α5-GABAR

component of inhibition and the NMDAR component of excitation increase with depolarization (Schulz et al., 2018). Hence the suppressive effect of α5-GABARs, both by hyperpolarizing the membrane potential and shunting the membrane conductance, is particularly strong when high frequency trains of presynaptic firing result in temporal summation of IPSPs. In effect, α5-GABARs function as anti-NMDARs.

After an initial episode of LTP, synaptic stimuli that previously produced only a brief depolarization can elicit a long-lasting plateau potential, including repetitive spiking. However, this regenerative response is revealed only when α5-GABARs are blocked, demonstrating the critical role these receptors acquire after synaptic redistribution. The appearance of a regenerative postsynaptic response should not be surprising, as the AMPAR-mediated depolarization is increased because of receptor insertion, the NMDAR-mediated depolarization is increased because of Mg^{2+} unblock and both of these events should lead to increased activation of depolarizing voltage-gated ion channels (Debanne et al., 2019). However, the suppression of the regenerative response by α5-GABARs and the ability of these receptors to suppress further induction of LTP was unexpected.

There are several steps in this process that are not yet fully understood. Our findings support the conclusion that dephosphorylation of radixin is the key activity-dependent event that dislodges α5-GABARs from extrasynaptic sites. However, the enzymatic steps underlying this process remain unclear. Excitatory synaptic activity leads to an increase in cytoplasmic Ca^{2+} and radixin-family proteins are substrates for several directly- or indirectly-Ca^{2+} regulated protein kinases and phosphatases (Kim et al., 2010; Siddoway et al., 2013), but which is responsible for α5-GABAR redistribution is unclear. Once redistribution occurs, α5-GABARs may mix freely with other isoforms within the synapse, or they might remain at the periphery of the synapse. The spatial relationship between synapses that have incorporated α5-GABARs and their metaplastic effects on excitatory synapses remains unknown. Presumably, this parameter determines the degree of synapse specificity for suppression of cumulative LTP. Finally, while we have demonstrated the importance of α5-GABARs for reversal learning, we do not yet understand all the steps in this process, nor its contribution to more complex forms of learning.

The critical role of α5-GABARs in regulating metaplasticity has remained hidden, despite decades of research on the fundamental mechanisms of excitatory and inhibitory synaptic plasticity. The revelations reported here depended critically on three aspects of our experimental approach. First, the development of an optogenetic pharmacology toolkit (Kramer et al., 2013), including azobenzene photoswitches and complementary receptor proteins, enabled unambiguous light-sensitive control of specific $GABA_A$ receptor isoforms. As part of this toolkit, our creation of knock-in mice expressing endogenous photosensitizable receptors ensured that the metaplasticity events we discovered are physiologically relevant. Second, we allowed excitatory and inhibitory synaptic events to interact in the voltage domain, without pharmacological blockade and outside of the influence of voltage clamp control, revealing how they dynamically influence membrane potential during and after induction of long-term plasticity. Third, by applying repeated episodes of high frequency stimulation, we revealed the metaplasticity that is controlled by α5-GABAR. These three experimental conditions not only made our discoveries possible,

but they are reflective of events *in vivo*, including when learning occurs during continual interaction of an animal with its environment.

Normal functioning requires a balance between stability of learned associations and behavioral flexibility. Consolidation of memory involves the transfer of information from hippocampus to neocortex, new protein synthesis ,and structural neuronal plasticity (Bailey et al., 2015). But first, there must be mechanisms that sustain memories in the short-term, despite the destabilizing influence of positive feedback. Our findings suggest that by freezing synaptic strength, the activity-dependent migration of α5-GABARs to synapses may be a critical early step in stabilizing learned associations until more durable events can lay down a long-term memory trace.

STAR Methods

Resource Availability

Lead Contact—Further information and requests for resources and reagents should be directed to and will be fulfilled by the lead contact, Richard H. Kramer (rhkramer@berkeley.edu).

Materials Availability—All unique/stable reagents generated in this study are available from the lead contact without restriction.

Data and Code Availability—The data supporting the current study have not been deposited in a public repository due to the idiosyncrasies of electrophysiological recordings, but are available from the lead contact on request.

Experimental Model and Subject Details

Mice—All experimental procedures were approved by the University of California Berkeley Animal Care and Use Committee, in compliance with all relevant regulatory standards.

Unless otherwise noted, mice were group housed by sex with free access to food and water. Mice aged 2 weeks - 6 months were used as indicated. Mice of both sex were used for electrophysiology experiments, and no influence of sex was observed on any results. Male mice were used for behavioral experiments, and were food restricted for 2 days prior to behavioral testing.

Mouse strains used in this study include C57BL/6J, referred to as wild type (WT) either obtained from Jackson Laboratory, or as litter-mate controls from genetically modified strain breeding; α1-GABAR-E125C knock in mice, referred to as α1-E125C-KI, generated by Lin et al., 2015, since deposited and available from Jackson Laboratory; α5-GABAR-E125C knock in mice, referred to as α5-E125C-KI, generated in this paper by the UC Davis mouse biology program; SOM-Cre-α5-E125C-KI mice generated by crossing SST-IRES-CRE mice from Jackson Laboratory with α5-E125C mice; PV-Cre-α5-E125C-KI mice generated by crossing PV-IRES-CRE mice obtained from Jackson Laboratory with α5-E125C mice; α5-GABAR knockout mice (α5-KO) obtained from Uwe Rudolph at McLean Hospital, under agreement with the University of Zurich.

Methods Details

α5-E125C knock-in mice were generated via the UC Davis mouse biology program. The genomic region of Gabra5 (NM_176942.4) was obtained from BAC clone RPCI-24 and was used to develop a targeting vector that contains the genomic region surrounding exons 5 and 6 of Gabra5. We introduced a cysteine mutation for T152 (counting from the start codon) on exon 5 as well as a C to T silent mutation to create a Hind III site upstream of T152C for genotyping. The construct was linearized and electroporated into ES cells from mouse strain 129. Cells were selected for transmitted neomycin resistance and homologous recombination was confirmed on flanking regions of the targeting vector. A loss of allele assay was performed to confirm a single recombination event. After karyotyping, ES cells were injected into C57/B6 mouse blastocysts and implanted into surrogates resulting in chimeras. After confirming germline transmission the F2 offspring were bred with a Cre recombinase expressing mouse to excise the neomycin cassette. The resulting progeny were bred to homozygosity of the Gabra5 knock-in and the Cre cassette was bred out.

SOM-Cre-α5-E125C-KI and PV-Cre-α5-E125C-KI were created by crossing SST-IRES-cre line (JAX stock 013044) and PV-IRES-cre line (JAX stock #008069), with α5-E125C-KI mice respectively.

Western Blot Analysis—Western blot analysis was performed by Raybiotech, Inc., using the automated Capillary Electrophoresis Immunoassay machine (WES™, ProteinSimple Santa Clara, CA) according to the manufacturer's protocol (Gentalen and Proctor, 2015; Rustandi et al., 2013). In brief, 0.6ug of samples were mixed with a master mix (ProteinSimple) to a final concentration of 1x sample buffer, 1x fluorescent molecular weight markers, and 40mM dithiothreitol (DTT) and then heated at 95°C for 5 min. The samples, blocking reagent, wash buffer, primary antibodies, secondary antibodies, and chemiluminescent substrate were dispensed into designated wells in the manufacturer provided microplate. After plate loading, the separation electrophoresis and immunodetection steps took place in the capillary system and were fully automated. Western analysis was carried out at room temperature, and instrument default settings were used. The data was analyzed with inbuilt Compass software (Proteinsimple).

Immunohistochemistry—After being deeply anesthetized with ketamine and xylazine, wide-type, α5-E125C-KI & α5-KO mice (8–12 weeks) were perfusion-fixed with 2% paraformaldehyde in 0.1 M sodium acetate buffer (pH. 6) and post-fixed in the same solution for 2–4 h. The brains were transferred to 30% sucrose in 0.9% saline overnight for cryoprotection. 18 Sagittal sections (40 μm) were sliced using a microtome. Free-floating slices were incubated with TBS (0.05 M Tris and 0.15 M NaCl; pH 7.4) containing 10% normal goat serum (NGS) (Jackson ImmunoResearch) for 1 h at room temperature. After blocking, slices were incubated with mouse anti-GABAAR α5 (diluted 1:500; Abcam, Rabbit polyclonal) in TBS with 2% NGS and 0.1% Triton X-100 at room temperature overnight. After three washes with TBS, slices were incubated with Alexa 546-conjugated secondary goat anti-rabbit antibody (1:500; Invitrogen) in TBS for 2 h at room temperature. After washing off residual secondary antibody, slices were mounted with anti-fade reagent (Vectorshield; Vector Labs). Digital images were acquired using a 5x objective on a Zeiss

microscope using a LED light source. The fluorescence intensity data were measured using a 10-pixel width line (region of interests, ROI) drawing across to the anatomical landmarks on the images from wide-type, knock-in & knock out brain sections. Data were processed and analyzed using ImageJ.

Viral Constructs—For over-expression of α5-GABARs, a bi-cistronic pAAV9 construct encoding the mutant α5(E125C) and a eGFP marker under control of the human synapsin-1 promoter was prepared as previously described (Lin et al., 2015).

EGFP-GFE3 was constructed by fusing the gene for enhanced green fluorescent protein (EGFP) 5' to a DNA sequence encoding a flexible linker of glycine-glycine-glycine-serine, repeated four times, and the gene for GFE3 (Gross et al., 2016), which consists of a FingR to Gephyrin (Gross et al., 2013) fused 5' to three consecutive HA-tags followed by amino acids 440-496 of the RING domain of rat XIAP (X-linked inhibitor of apoptosis). To constitutively express GFE3 by Cre-induction in AAV transduced neurons, EGFP-GFE3 was subcloned into the MCS of the pAAV-EF1a-DIO (Saunders et al., 2012) vector.

AAV-flex-ReaChR-citrine DNA was obtained from Addgene (catalog #50955). The DNA clones were subsequently packaged into AAV9 at a titer of 10^{12}–10^{14} vg/mL.

Radixin-T564A and Radixin-T564D were obtained by insertion of a single point mutation at T546 in Radixin-WT DNA using the Quikchange mutagenesis kit (Agilent). The DNA clones were subsequently packaged into AAV9 at a titer of 10^{12}–10^{14} vg/mL.

Viruses were injected into the dorsal hippocampus in neonatal mice. Recordings were performed 3-4 weeks later. GFP positive CA1 pyramidal neurons were targeted for whole cell recording.

Electrophysiology—For acute hippocampal and dentate gyrus slice, mice of both sexes were anaesthetized with isoflurane and decapitated. Brains were removed and placed in ice cold slicing solution containing (in mM) 85 NaCl, 2.5 KCl, 0.5 $CaCl_2$, 4 $MgCl_2$, 1.25 NaH_2PO_4, 26 $NaHCO_3$, 75 sucrose, 0.5 ascorbic acid and 10 glucose (saturated with 95% O_2 and 5% CO_2; pH 7.4). 400 micron coronal slices were made using a vibrating microtome (Leica). Slices were transferred to 34 °C artificial cerebrospinal fluid (ACSF) containing 126 NaCl, 2.5 KCl, 2.5 $CaCl_2$, 1.3 $MgCl_2$, 1.25 NaH_2PO_4, 26 $NaHCO_3$and 10 glucose (saturated with 95% O_2 and 5% CO_2; 290-300 mOsm; pH 7.4). After 30 min, slices were allowed to recover for 1 hr at room temperature. Slices were placed on the stage of an upright microscope (Olympus) and perfused with ACSF at 1-2 ml/min at 30-32 °C.

For photoswitch treatment, after recovery slices were incubated in ACSF with TCEP (5 mM, 5–10 min), washed, and then incubated with PAG1C (25–50 μM, with 500 μM guanidinium hydrochloride) for 45-60 min at room temperature. 540 nm (15 mW/cm^2) or 390 nm (3.5 mW/cm^2) light was generated by a Spectra-X LED light source (Lumencor) triggered by software and delivered via the microscope optical port through a 20X objective. At this intensity maximal photoswitching occurs in ~ 200 ms (Lin et al., 2015). To ensure maximal photoswitching, light was applied at least 1 s before any measurement (see individual experiments for details).

For field recordings, acute brain slices were prepared as described above from 2-6 month old mice. A glass stimulating electrode (2-6 mohm) filled with ACSF was placed in stratum radiatum ~ 500 μm from the recording electrode and current pulses 0.033 Hz, 10-100 microamp, 0.2 ms were delivered by a stimulus isolation unit (isoflex, AMPI) triggered by recording software. A glass recording electrode (2-6 MΩ) filled with ACSF was placed in stratum radiatum and voltage was amplified, digitized, and recorded to the computer.

For LTP experiments stimulation intensity was set so the initial slope of the fEPSP was approximately half the slope at the threshold for eliciting a population spike. Recordings were discarded if the slope drifted more than 10% over the last 10 minutes of baseline recording. LTP was induced by theta burst stimulation (TBS): 5 stimuli at 100 Hz, repeated 5 times every 250 ms. LTP was quantified as the ratio of the initial fEPSP slope 20 minutes after TBS delivery to the initial fEPSP slope during the final minute of baseline. Slopes used for quantification were the average of several consecutive trials. LTD was induced by 900 stimuli at 1Hz, or 100 stimuli at 10 Hz. Light was on from ~5 s before to ~5 s after TBS or 10 Hz stimulation. During 1 Hz stimulation, light was pulsed on 1s every 2 min. TB-21007 (Tocris) was prepared as a 5 mM stock in DMSO and diluted to final concentration in ACSF.

For whole cell recordings, acute brain slices were prepared as described above from 2-3 week old mice. Slices were visualized with DODT contrast infrared optics (Luigs and Neumann). CA1 pyramidal neurons were targeted for whole cell recording with glass electrodes (4-6 MOhm) filled with 108 Cs-gluconate, 2.8 NaCl, 20 HEPES, 5 TEA-Cl, 0.4 EGTA, 4 Mg-ATP, 0.3 Na-GTP, 10 phosphocreatine; 290 mOsm; pH 7.2 for voltage clamp recordings, and with 116 K-gluconate, 20 HEPES, 6 KCl, 2NaCl, 0.5 EGTA, 4 Mg-ATP, 0.3 Na-GTP, 10 phosphocreatine; 290 mOsm; pH 7.2 for current clamp recordings. For whole cell LTP experiments (Figure 6) Mg-ATP, Na-GTP and phosphocreatine were added fresh on each day of recording. Input resistance, series resistance (in voltage clamp), and membrane voltage (in current clamp) were monitored throughout recording to ensure stable recording quality and cell health. Pipette capacitance was compensated. In current clamp, series resistance was < 20 MΩ and was compensated with the amplifier's bridge balance circuit. In voltage clamp recordings series resistance was < 20 MΩ and was uncompensated. For examining whole cell effects of LTP, the following TBS protocol was used: 10 stimuli at 100 Hz, repeated 10 times every 250 ms.

Phasic IPSCs were recorded by holding the neurons at 0 mV and delivering single stimuli repeated at 0.2 Hz or trains of stimuli (5 at 100 Hz) repeated at 0.1 Hz. Monosynaptic IPSCs were recorded in the presence of 50 μM APV and 10 μM DNQX, or 3 mM kynurenic acid. The effect of light was assessed by measuring the IPSC peak or area after 1 s of illumination with 390 nm and 540 nm light on alternating trials. 5-10 trials were averaged for each wavelength and photo-block was calculated as $1-(I_{540}/I_{390})$.

Tonic GABAergic currents were recorded in the presence of 1 μM TTX and either 50 μM APV and 10 μM DNQX or 3 mM kynurenic acid. 40-50 mL of ACSF was recirculated to avoid washout of ambient GABA. One second 540 and 390 nm light pulses were alternated every 5 s. Tonic current amplitude was calculated from the peak of a gaussian curve fit to the

negative half of a histogram of all current values over 1 s of recording (Bright and Smart, 2013).

For whole cell LTP (Figure 6), baseline was limited to 5 min. Response amplitude was measured as the initial slope of the depolarizing PSP with the cell at rest. LTP was quantified as the ratio of the response ~ 20 min after TBS delivery to the response during baseline. E/I Ratio was calculated by dividing the depolarizing PSP peak with the cell at rest (~−65 mV) and the hyperpolarizing PSP peak with the cell depolarized to ~−55 mV by current injection.

For cLTP (Figure S4): 20 μM NMDA was bath applied for 2 minutes and rapidly washed out (adopted from Chiu et al., 2018).

Electrophysiological recordings were collected using WinLTP (WinLTP Ltd.) or pCLAMP (Molecular Devices) software and were analyzed using Excel (Microsoft), pCLAMP, Igor (Wavemetrics), and Sigmaplot (Systat).

For optogenetic stimulation of ReChR, we used a red LED (wavelength: 625 nm, 17.5 mW; Thorlabs) controlled by digital outputs.

Behavior—Stereotaxic injections were performed on male mice 8-12 weeks old as previously described (Lammel et al., 2008; Lammel et al., 2012; Lammel et al., 2015), under general ketamine–dexmedetomidine anesthesia and using a stereotaxic instrument (Kopf Instruments, Model 1900). One layer of adhesive cement (C&B Metabond; Parkell) followed by cranioplastic cement (Dental cement) was used to secure the fiber to the skull. The incision was closed with a suture and tissue adhesive (Vetbond; 3M). The animal was kept on a heating pad until it recovered from anesthesia. Experiments were performed 7 days after implanting a double guide injection cannula (coordinates were x: 1.3, y: −1.68 and Z: −1.6, distance between the two guide is 2.6 mm). Cannula placements were confirmed by preparing coronal sections (50-100 mm) of implantation sites after the behavior experiment.

For reversal learning, trials were conducted in operant conditioning chambers (24 cm W x 20 cm D x 18 cm H, Med Associates) contained within a sound-attenuating cabinet. The right side of the chamber was fitted with two nose poke ports, each with an LED light at the rear. Reward delivery (sugar pellet) was controlled by a computer running Med PC IV software (Med Associates), which also recorded nose poke responses. The day before the learning trial, the mice spent two 15 min shaping trials in the chamber to habituate to the environment and recover from handling. During the shaping trial, both left and right nose pokes were active and the mice also learn to associate nose poke with sugar pellet reward. The start of any trial was indicated to the mouse by the illumination of a white house light. The shaping trial is followed by learning trials the following days during which time mice were free to respond at the two nose poke ports. One port was designated the “active” port, and a response at this port was rewarded with a sugar pellet. Each mouse underwent 2 learning trials (15 mins) per day for 3 continuous days. During the reversal learning trials, the port designated the “active” port was made “inactive” and the other port was designated the “active” port. Each mouse underwent 6 reversal learning trials (15 mins) in one day. All

the “active” and “inactive” nose poke responses were recorded and the percentage correct response was obtained for each mouse.

For drug injection, an internal cannula was connected to a 5 μl Hamilton syringe via a thin tubing. PAG1C - We bilaterally injected 1 μl ACSF containing 250 μM of PAG1C + 500 μM of TCEP through the implanted cannula an hour before reversal learning trial R-1; Saline control - We bilaterally injected 1 μl ACSF containing 500 μM of TCEP bilaterally through the implanted cannula an hour before reversal learning trial R-1; APV - We bilaterally injected 1 μl of ACSF containing 100 μM of APV an hour before reversal learning trial R-1.

Mice were on a restricted diet 2 days prior to the start of the behavior until the end of the behaviour. Each mouse was provided 1.5 g of food for every 25 g of their body weight. There was no water restriction.

Quantification and Statistical Analysis

Unless otherwise noted, all reported values in text and figures are mean ± standard error. Statistical tests were performed as indicated in the text. All distributions were tested for normality (Shapiro-Wilk test) and equal variance. If normal, a two-tailed Student’s t-test was performed. If non-normal a Mann-Whitney Rank Sum test was performed. For behavioural experiments, one way ANOVA was used to compare multiple groups. Significance was defined as $p < 0.05$.

Supplementary Material

Refer to Web version on PubMed Central for supplementary material.

Acknowledgements

This research was supported by the National Institutes of Health grant R01NS100911 to R.H.K.. We thank Neil Wilson, Seyedeh Atiyeh Afjei and Brian Hitchin for technical assistance, Wan-Chen Lin for synthesizing PAG1C, Uwe Rudolph for providing α5-GABAR knockout mice, Daniel E. Feldman and Steven A. Siegelbaum for critical comments on this manuscript, and Stanislav S. Zakharenko for use of equipment and time.

References

Abraham WC, Bear MF (1996) Metaplasticity: the plasticity of synaptic plasticity. Trends in Neurosciences 19 (4), 126–130. [PubMed: 8658594]

Bailey CH, Kandel ER, and Harris KM (2015). Structural Components of Synaptic Plasticity and Memory Consolidation. Cold Spring Harbor Perspectives in Biology 7.

Berretta N, and Jones RSG (1996). Tonic facilitation of glutamate release by presynaptic N-methyl-d-aspartate autoreceptors in the entorhinal cortex. Neuroscience 75, 339–344. [PubMed: 8931000]

Bezaire MJ, and Soltesz I (2013). Quantitative assessment of CA1 local circuits: Knowledge base for interneuron-pyramidal cell connectivity. Hippocampus 23, 751–785. [PubMed: 23674373]

Bliss T, and Collingridge GL (2019). Persistent memories of long-term potentiation and the N-methyl-d-aspartate receptor. Brain and Neuroscience Advances 3, 1–10.

Brady ML, and Jacob TC (2015). Synaptic localization of α5 GABA (A) receptors via gephyrin interaction regulates dendritic outgrowth and spine maturation. Developmental neurobiology 75(11), 1241–1251. [PubMed: 25663431]

Brickley SG, Revilla V, Cull-Candy SG, Wisden W, Farrant M (2001). Adaptive regulation of neuronal excitability by a voltage-independent potassium conductance. Nature 409, 88–92. [PubMed: 11343119]

Bright D, and Smart TG (2013). Methods for recording and measuring tonic GABAA receptor-mediated inhibition. Frontiers in Neural Circuits 7, 193. [PubMed: 24367296]

Brünig I, Scotti E, Sidler C, and Fritschy J-M (2002). Intact sorting, targeting, and clustering of γ-aminobutyric acid A receptor subtypes in hippocampal neurons in vitro. The Journal of Comparative Neurology 443, 43–55. [PubMed: 11793346]

Buszáki G (1984). Feed-forward inhibition in the hippocampal formation. Prog. Neurobiol 22, 131–153. [PubMed: 6433403]

Caraiscos VB, Elliott EM, You-Ten KE, Cheng VY, Belelli D, Newell JG, Jackson MF, Lambert JJ, Rosahl TW, Wafford KA, et al. (2004). Tonic inhibition in mouse hippocampal CA1 pyramidal neurons is mediated by alpha5 subunit-containing gamma-aminobutyric acid type A receptors. Proc Natl Acad Sci U S A 101, 3662–3667. [PubMed: 14993607]

Castillo PE, Chiu CQ, and Carroll RC (2011). Long-term plasticity at inhibitory synapses. Current Opinion in Neurobiology 21, 328–338. [PubMed: 21334194]

Chevaleyre V, and Castillo PE (2004). Endocannabinoid-Mediated Metaplasticity in the Hippocampus. Neuron, 43(6), 871–881. [PubMed: 15363397]

Chiu CQ, Martenson JS, Yamazaki M, Natsume R, Sakimura K, Tomita S, Tavalin SJ, and Higley MJ (2018). Input-Specific NMDAR-Dependent Potentiation of Dendritic GABAergic Inhibition. Neuron 97(2), 368–377. [PubMed: 29346754]

Collinson N, Kuenzi FM, Jarolimek W, Maubach KA, Cothliff R, Sur C, Smith A, Otu FM, Howell O, Atack JR, et al. (2002). Enhanced Learning and Memory and Altered GABAergic Synaptic Transmission in Mice Lacking the α5 Subunit of the GABAA Receptor. The Journal of Neuroscience 22, 5572–5580. [PubMed: 12097508]

Crestani F, Keist R, Fritschy J-M, Benke D, Vogt K, Prut L, Bluthmann H, Mohler H, and Rudolph U (2002). Trace fear conditioning involves hippocampal α5 GABAA receptors. Proceedings of the National Academy of Sciences 99, 8980–8985.

Davies SN, Collingridge GL. (1989). Role of excitatory amino acid receptors in synaptic transmission in area CA1 of rat hippocampus. Proceedings of the Royal Society of London: Series B, Biological Sciences 236, 373–384.

Dawson GR, Maubach KA, Collinson N, Cobain M, Everitt BJ, MacLeod AM, Choudhury HI, McDonald LM, Pillai G, Rycroft W, et al. (2006). An Inverse Agonist Selective for α5 Subunit-Containing GABAA Receptors Enhances Cognition. Journal of Pharmacology and Experimental Therapeutics 316, 1335–1345.

Debanne D, Inglebert Y, and Russier M (2019). Plasticity of intrinsic neuronal excitability. Current Opinion in Neurobiology 54, 73–82. [PubMed: 30243042]

Dunfield D, Haas K. (2009). Metaplasticity governs natural experience-driven plasticity of nascent embryonic brain circuits. Neuron. 2009;64(2):240–250. [PubMed: 19874791]

Fritschy J-M, and Mohler H (1995). GABAA-receptor heterogeneity in the adult rat brain: Differential regional and cellular distribution of seven major subunits. The Journal of Comparative Neurology 359, 154–194. [PubMed: 8557845]

Gentalen ET, and Proctor JM (2015). Using the Peggy Simple Western System for Fine Needle Aspirate Analysis In Apoptosis and Cancer: Methods and Protocols, Mor G, and Alvero AB, eds. (New York, NY: Springer New York), pp. 139–155.

Glykys J, and Mody I (2006). Hippocampal network hyperactivity after selective reduction of tonic inhibition in GABA A receptor alpha5 subunit-deficient mice. J Neurophysiol 95, 2796–2807. [PubMed: 16452257]

Gross GG, Junge JA, Mora RJ, Kwon H-B, Olson CA, Takahashi TT, Liman ER, Ellis-Davies GCR, McGee AW, Sabatini BL, et al. (2013). Recombinant Probes for Visualizing Endogenous Synaptic Proteins in Living Neurons. Neuron 78, 971–985. [PubMed: 23791193]

Gross GG, Straub C, Perez-Sanchez J, Dempsey WP, Junge JA, Roberts RW, Trinh LA, Fraser SE, De Koninck Y, De Koninck P, et al. (2016). An E3-ligase-based method for ablating inhibitory synapses. Nat Meth 13, 673–678.

Hausrat TJ, Muhia M, Gerrow K, Thomas P, Hirdes W, Tsukita S, Heisler FF, Herich L, Dubroqua S, Breiden P, et al. (2015). Radixin regulates synaptic GABAA receptor density and is essential for reversal learning and short-term memory. Nat Commun 6.

Hayama T, Noguchi J, Watanabe S, Takahashi N, Hayashi-Takagi A, Ellis-Davies GCR, Matsuzaki M, and Kasai H (2013). GABA promotes the competitive selection of dendritic spines by controlling local Ca2+ signaling. Nat Neurosci 16, 1409–1416. [PubMed: 23974706]

Huang YY, Colino A, Selig DK, and Malenka RC (1992). The influence of prior synaptic activity on the induction of long-term potentiation. Science, 255(5045), 730–733. [PubMed: 1346729]

Jahr CE (1994). NMDA receptor kinetics and synaptic function. Seminars in Neuroscience 6, 81–86.

Kasugai Y, Swinny JD, Roberts JD, Dalezios Y, Fukazawa Y, Sieghart W, Shigemoto R, and Somogyi P (2010). Quantitative localisation of synaptic and extrasynaptic GABAA receptor subunits on hippocampal pyramidal cells by freeze-fracture replica immunolabelling. The European Journal of Neuroscience 32(11), 1868–1888. [PubMed: 21073549]

Kim HS, Bae CD, Park J (2010). Glutamate receptor-mediated phosphorylation of ezrin/radixin/moesin proteins is implicated in filopodial protrusion of primary cultured hippocampal neuronal cells. J Neurochem. 113, 1565–1576. [PubMed: 20367752]

Kralic JE, Korpi ER, O'Buckley TK, Homanics GE, Morrow AL (2002). Molecular and pharmacological characterization of GABAA receptor α1 subunit knockout mice. J. Pharmacol. Exp. Ther 302, 1037–1045. [PubMed: 12183661]

Kramer RH, Mourot A, and Adesnik H (2013). Optogenetic pharmacology for control of native neuronal signaling proteins. Nat Neurosci 16, 816–823. [PubMed: 23799474]

Lammel S, Hetzel A, Häckel O, Jones I, Liss B, and Roeper J (2008). Unique Properties of Mesoprefrontal Neurons within a Dual Mesocorticolimbic Dopamine System. Neuron 57, 760–773. [PubMed: 18341995]

Lammel S, Lim BK, Ran C, Huang KW, Betley MJ, Tye KM, Deisseroth K, and Malenka RC (2012). Input-specific control of reward and aversion in the ventral tegmental area. Nature 491, 212. [PubMed: 23064228]

Lammel S, Steinberg, Elizabeth E, Földy C, Wall, Nicholas R, Beier K, Luo L, and Malenka, Robert C (2015). Diversity of Transgenic Mouse Models for Selective Targeting of Midbrain Dopamine Neurons. Neuron 85, 429–438. [PubMed: 25611513]

Laughlin RE, Grant TL, Williams RW, and Jentsch JD (2011). Genetic Dissection of Behavioral Flexibility: Reversal Learning in Mice. Biological Psychiatry 69, 1109–1116. [PubMed: 21392734]

Lin W-C, Tsai M-C, Davenport, Christopher M, Smith, Caleb M, Veit J, Wilson, Neil M, Adesnik H, and Kramer, Richard H (2015). A Comprehensive Optogenetic Pharmacology Toolkit for In Vivo Control of GABAA Receptors and Synaptic Inhibition. Neuron 88, 879–891. [PubMed: 26606997]

Loebrich S, Bahring R, Katsuno T, Tsukita S, and Kneussel M (2006). Activated radixin is essential for GABAA receptor α5 subunit anchoring at the actin cytoskeleton. EMBO J 25, 987–999. [PubMed: 16467845]

Malinow R, and Tsien RW (1990). Presynaptic enhancement shown by whole-cell recordings of long-term potentiation in hippocampal slices. Nature 346, 177. [PubMed: 2164158]

Matsui T, Maeda M, Doi Y, et al. (1998). Rho-kinase phosphorylates COOH-terminal threonines of ezrin/radixin/moesin (ERM) proteins and regulates their head-to-tail association. J Cell Biol. 140:647–657. [PubMed: 9456324]

Mayer ML, Westbrook GL, and Guthrie PB (1984). Voltage-dependent block by Mg2+ of NMDA responses in spinal cord neurones. Nature 309, 261. [PubMed: 6325946]

Moss SJ, Smart TG. Constructing inhibitory synapses. Nat Rev Neurosci. 2001;2(4):240–250. [PubMed: 11283747]

Mourot A, Kienzler MA, Banghart MR, et al. (2011). Tuning photochromic ion channel blockers. ACS Chem Neurosci.;2:536–543. [PubMed: 22860175]

Nicoll RA (2017). A Brief History of Long-Term Potentiation. Neuron 93, 281–290. [PubMed: 28103477]

Papouin T, Ladepeche L, Ruel J.r.m., Sacchi S, Labasque M, Hanini M, Groc L, Pollegioni L, Mothet J-P, and Oliet S.p.H.R. (2012). Synaptic and Extrasynaptic NMDA Receptors Are Gated by Different Endogenous Co-agonists. Cell 150, 633–646. [PubMed: 22863013]

Pelkey KA, Chittajallu R, Craig MT, Tricoire L, Wester JC, McBain CJ (2017). Hippocampal GABAergic Inhibitory Interneurons. Physiological Reviews. 97, 1619. [PubMed: 28954853]

Pelletier JG, and Lacaille J-C (2008). Chapter 14 Long-term synaptic plasticity in hippocampal feedback inhibitory networks In Progress in Brain Research, Sossin WS, Lacaille J-C, Castellucci VF, and Belleville S, eds. (Elsevier), pp. 241–250.

Picton AJ, and Fisher JL (2007). Effect of the alpha subunit subtype on the macroscopic kinetic properties of recombinant GABA(A) receptors. Brain research 1165, 40–49. [PubMed: 17658489]

Ponomarev I, Maiya R, Harnett MT, Schafer GL, Ryabinin AE, Blednov YA, Morikawa H, Boehm SL, Homanics GE, Berman A, et al. (2006). Transcriptional signatures of cellular plasticity in mice lacking the α1 subunit of GABAA receptors. Journal of Neuroscience 26, 5673–5683. [PubMed: 16723524]

Prenosil GA, Schneider Gasser EM, Rudolph U, Keist R, Fritschy JM, Vogt KE (2006). Specific subtypes of GABAA receptors mediate phasic and tonic forms of inhibition in hippocampal pyramidal neurons. Journal of Neurophysiology 96, 846–857. [PubMed: 16835366]

Rudolph U, and Möhler H (2014). $GABA_A$ receptor subtypes: Therapeutic potential in Down syndrome, affective disorders, schizophrenia, and autism. Annual review of pharmacology and toxicology 54, 483–507.

Rusakov DA, Scimemi A, Walker MC, and Kullmann DM (2004). Comment on Role of NMDA Receptor Subtypes in Governing the Direction of Hippocampal Synaptic Plasticity. Science 305, 1912. [PubMed: 15448254]

Rustandi RR, Anderson C, and Hamm M (2013). Application of Capillary Electrophoresis in Glycoprotein Analysis In Glycosylation Engineering of Biopharmaceuticals: Methods and Protocols, A. Beck, ed. (Totowa, NJ: Humana Press), pp. 181–197.

Saliba RS, Michels G, Jacob TC, Pangalos MN, and Moss SJ (2007). Activity-Dependent Ubiquitination of GABAA Receptors Regulates Their Accumulation at Synaptic Sites. The Journal of Neuroscience 27, 13341. [PubMed: 18045928]

Saunders A, Johnson C, and Sabatini B (2012). Novel recombinant adeno-associated viruses for Cre activated and inactivated transgene expression in neurons. Frontiers in Neural Circuits 6, 47. [PubMed: 22866029]

Schulz JM, Knoflach F, Hernandez M-C, and Bischofberger J (2018). Dendrite-targeting interneurons control synaptic NMDA-receptor activation via nonlinear α5-GABAA receptors. Nature Communications 9, 3576.

Serwanski DR, Miralles CP, Christie SB, Mehta AK, Li X, and De Blas AL (2006). Synaptic and nonsynaptic localization of GABAA receptors containing the α5 subunit in the rat brain. The Journal of Comparative Neurology 499, 458–470. [PubMed: 16998906]

Siddoway BA, Altimimi HF, Hou H, Petralia RS, Xu B, Stellwagen D, Xia H (2013). An essential role for Inhibitor-2 regulation of Protein Phosphatase-1 in synaptic scaling. Journal of Neuroscience 33, 11206–11211. [PubMed: 23825423]

Sieghart W, Fuchs K, Tretter V, Ebert V, Jechlinger M, H√∂ger H, and Adamiker D (1999). Structure and subunit composition of GABAA receptors. Neurochemistry International 34, 379–385. [PubMed: 10397365]

Sieghart W, and Sperk G (2002). Subunit Composition, Distribution and Function of GABA-A Receptor Subtypes. Current Topics in Medicinal Chemistry 2, 795. [PubMed: 12171572]

Takeuchi T, Duszkiewicz AJ, and Morris RGM (2014). The synaptic plasticity and memory hypothesis: encoding, storage and persistence. Philosophical Transactions of the Royal Society B: Biological Sciences 369.

Thomson AM, Bannister AP, Hughes DI, and Pawelzik H (2000). Differential sensitivity to Zolpidem of IPSPs activated by morphologically identified CA1 interneurons in slices of rat hippocampus. European Journal of Neuroscience 12, 425–436

Toda T and Gage FH. (2018). Review: adult neurogenesis contributes to hippocampal plasticity. Cell Tissue Res. 373:693–709. [PubMed: 29185071]

Tretter VE, Mukherjee J, Maric HM, Schindelin H, Sieghart W, and Moss SJ (2012). Gephyrin, the enigmatic organizer at GABAergic synapses. Frontiers in Cellular Neuroscience 6, 23. [PubMed: 22615685]

Vose LR, and Stanton PK (2017). Synaptic Plasticity, Metaplasticity and Depression. Current neuropharmacology 15(1), 71–86. [PubMed: 26830964]

Wang L and Maffei A (2014) Inhibitory Plasticity Dictates the Sign of Plasticity at Excitatory Synapses. The Journal of Neuroscience 34, 1083–1093. [PubMed: 24453301]

Weir CJ, Mitchell SJ, and Lambert JJ (2017). Role of GABAA receptor subtypes in the behavioural effects of intravenous general anaesthetics. BJA: British Journal of Anaesthesia 119, i167–i175. [PubMed: 29161398]

Wigstrom H, and Gustafsson B (1983). Facilitated induction of hippocampal long-lasting potentiation during blockade of inhibition. Nature 301, 603–604. [PubMed: 6298626]

Xu J, Antion MD, Nomura T, Kraniotis S, Zhu Y, Contractor A. (2014). Hippocampal metaplasticity is required for the formation of temporal associative memories. J Neurosci. 34:16762–16773. [PubMed: 25505329]

Zarnowska ED, Keist R, Rudolph U, and Pearce RA (2009). GABAA Receptor α5 Subunits Contribute to GABAA slow Synaptic Inhibition in Mouse Hippocampus. Journal of Neurophysiology 101, 1179–1191. [PubMed: 19073796]

Zorumski CF, and Izumi Y (2012). NMDA receptors and metaplasticity: Mechanisms and possible roles in neuropsychiatric disorders. Neuroscience and Biobehavioral Reviews 36, 989–1000. [PubMed: 22230702]

Highlights

- Optical control of endogenous $GABA_A$ receptors containing the α5 subunit
- Excitatory activity redistributes extrasynaptic α5-GABARs to inhibitory synapses
- α5-GABARs prevent runaway hippocampal excitatory LTP
- α5-GABARs preserve learned associations in mice

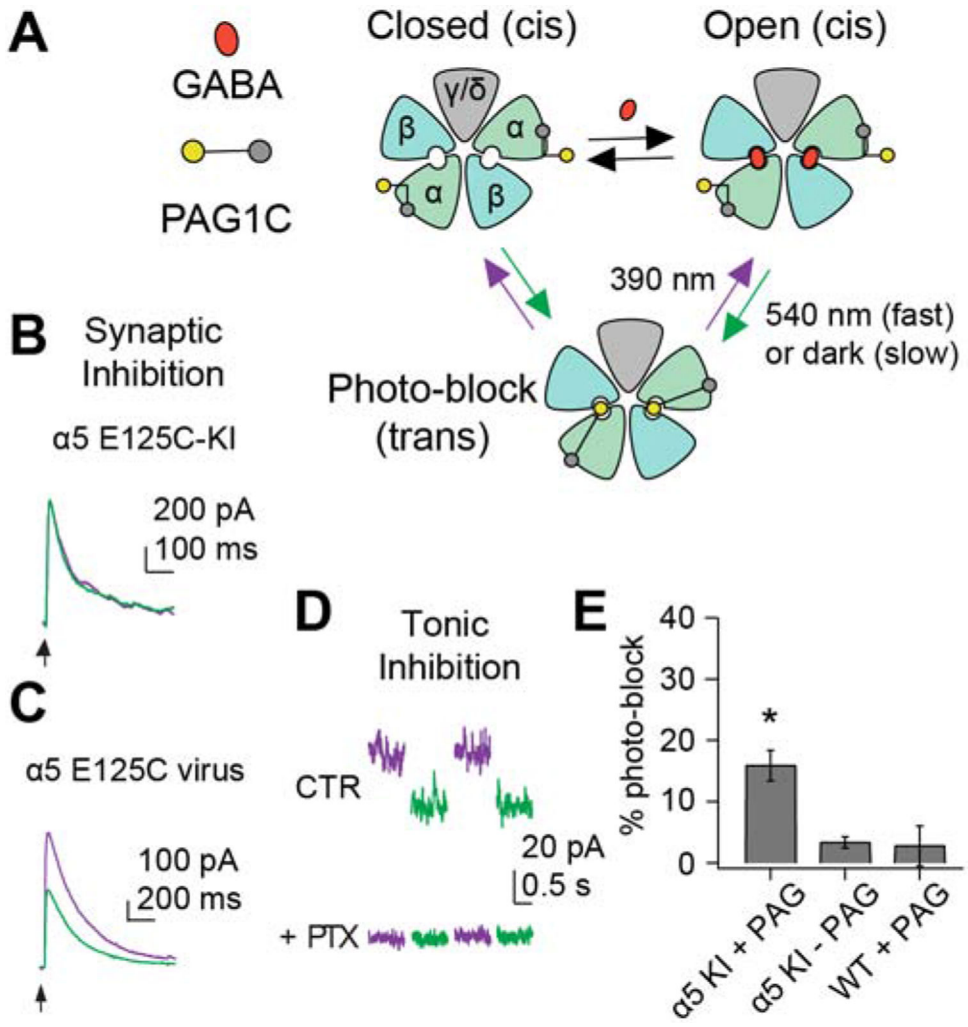

Figure 1. Photo-block reveals the role of endogenous α5-GABARs in synaptic and tonic inhibition.

A. Attachment of PAG1C to the α5 subunit photosensitizes endogenous α5-GABARs. In *trans*, PAG1C reaches the GABA binding site, competing with free GABA to prevent activation. PAG1C switches to *cis* in 390 nm light, vacating the site and restoring receptor function. PAG1C relaxes to *trans* slowly in darkness or rapidly in 540 nm light.

B. Photo-block is imposed by switching between 390 nm (purple traces) to 540 nm (green trace). At rest, photo-bock had no effect on IPSCs, indicating that endogenous α5-GABARs do not contribute to synaptic inhibition. IPSCs were elicited by extracellular stimulation (arrow) in a hippocampal slice from an α5-E125C-KI mouse. N = 7 cells.

C. After viral overexpression of α5-E125C-GABAR,IPSCs could be photo-blocked, indicating increased synaptic contribution. N = 8 cells.

D. At rest, photo-block of α5-GABARs reduced holding current, indicating a contribution to tonic inhibition. Picrotoxin eliminated the effect of photo-block.

E. Group data showing contribution of α5-GABAR to tonic inhibition. N = 4 cells for each.

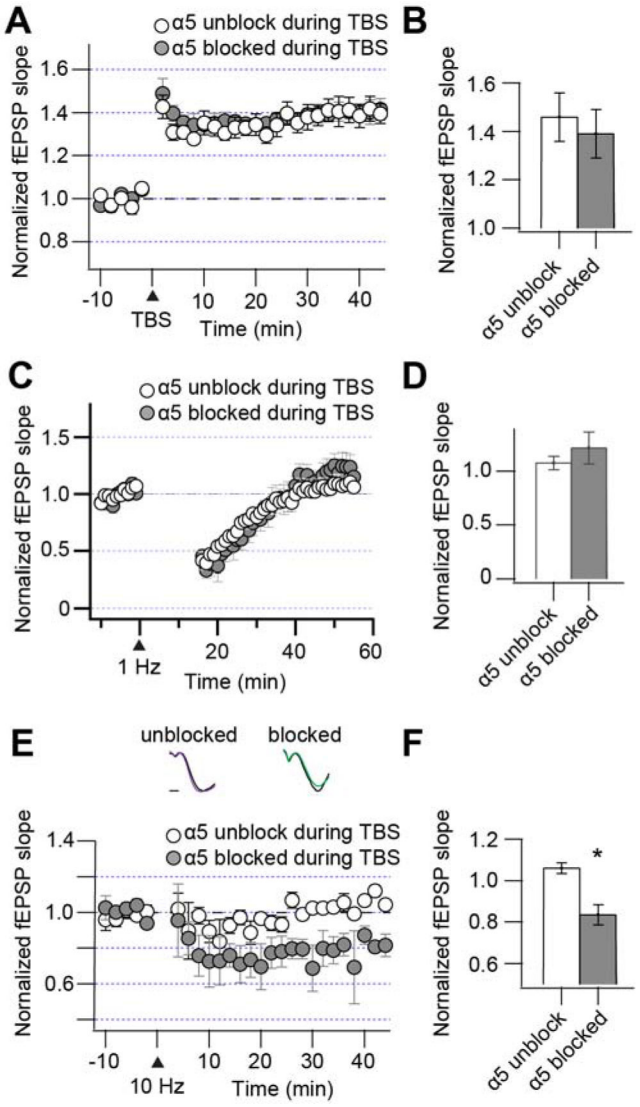

Figure 2. Photo-block of α5-GABARs suppresses induction of LTD but not LTP

A. LTP induced by theta burst stimulation (TBS; 5 stimuli at 100 Hz, 5 times every 250 ms; arrow) was unaffected by α5-GABAR photo-block. N = 5 slices from adult mice (P42-60).

B. Photo-block had no effect on mean LTP amplitude.

C. Low frequency stimulation (900 stimuli at 1 Hz; arrow) did not induce long term plasticity, and was unaffected by α5-GABAR photo-block. N = 5 slices.

D. Mean normalized fEPSP amplitude after 1 Hz stimulation with α5-GABARs unblocked (white) or blocked (grey).

E. 10 Hz stimulation (10 Hz, 10s; arrow) induced LTD when α5-GABARs were photo-blocked (gray), but not when they were unblocked (white). N = 4 slices. Example fEPSPs are shown above, normalized to the baseline trace (black). Horizontal scale bar = 5 ms.

F. Average LTD amplitude with α5-GABARs unblocked (white) or blocked (gray).

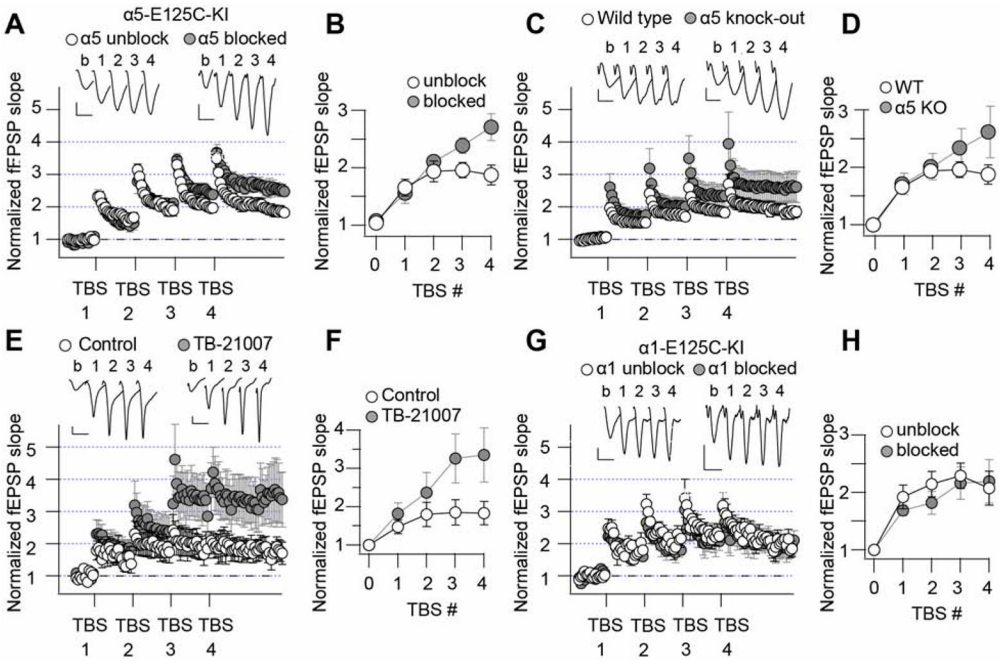

Figure 3. α5-GABARs suppress the accumulation of excitatory LTP.

A. Photo-block of α5-GABARs increases the accumulation of LTP. Synaptic inputs were stimulated with 4 TBS, delivered 20 min apart. LTP saturates more readily with α5-GABARs unblocked (white) vs photo-blocked (gray). N = 5 slices. Example fEPSP traces from baseline (b) and after each TBS are shown above the timecourse. Traces are shown after the stimulus artifact. The size of baseline traces is scaled between conditions to compare LTP.

B. LTP amplitude after each TBS with α5-GBARs unblocked (white) or blocked (gray).

C. Genetic knock-out of α5-GABARs suppresses accumulation of LTP. Synaptic inputs were stimulated with 4 TBS, delivered 20 min apart. LTP saturates more readily in WT (white) vs α5-KO mice (gray). N = 10 slices.

D. LTP amplitude after each TBS delivery in WT (white) and α5-KO mice (gray).

E. An α5-GABAR inverse agonist (TB-21007) enhances accumulation of LTP. Synaptic inputs were stimulated with 4 TBS, delivered 20 min apart. LTP saturates more readily in control (white) vs 5 nM TB-21007 (gray). N = 6 slices.

F. LTP amplitude after each TBS delivery in control (white) and with TB-21007 (gray).

G. Photo-block of α1-GABARs has no effect on accumulation of LTP. N = 5 slices.

H. LTP amplitude after each TBS delivery with α1-GABARs unblocked (white) or blocked (gray).

Scale bars in all panels = 0.2 mV, 10 ms.

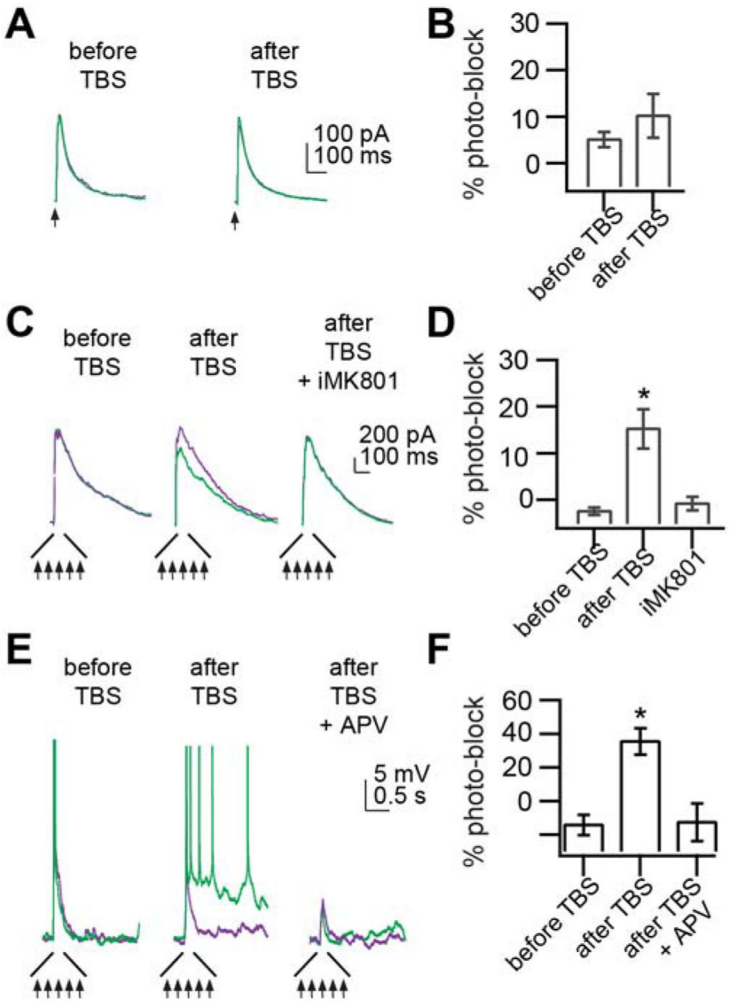

Figure 4. Theta burst stimulation increases inhibitory synaptic contribution of α5-GABARs, suppressing excitatory synaptic responses mediated by NMDARs.

A. IPSCs evoked by a single stimulus (arrow) were unaffected by α5-GABAR photo-block, consistent with absence from inhibitory synapses. Responses were recorded in separate cells in the same slice before or after TBS.

B. Quantification of the effect of α5-GABAR photo-block on single IPSCs. N = 7 cells for each condition.

C. IPSCs evoked by a brief train of stimuli (5 at 100 Hz; arrows) were affected by α5-GABAR photo-block, but only after TBS, consistent with activity-dependent relocation to inhibitory synapses. Responses before or after TBS were recorded in separate cells from the same slice. MK801 introduced via the patch pipette prevented activity-dependent photo-block of IPSCs (right).

D. Quantification of photo-block of IPSCs to a brief stimulus train. N = 4 cells for each condition.

E. Example postsynaptic voltage responses to a brief train of stimuli. Photo-block of α5-GABARs had no effect on the voltage response in cells sampled before TBS (left), but elicited a sustained depolarization in cells sampled after TBS. Blocking NMDARs with APV abolished the persistent depolarization and eliminated photosensitivity (right).

F. Quantification of photo-block of postsynaptic response area. N = 4 cells for each condition.

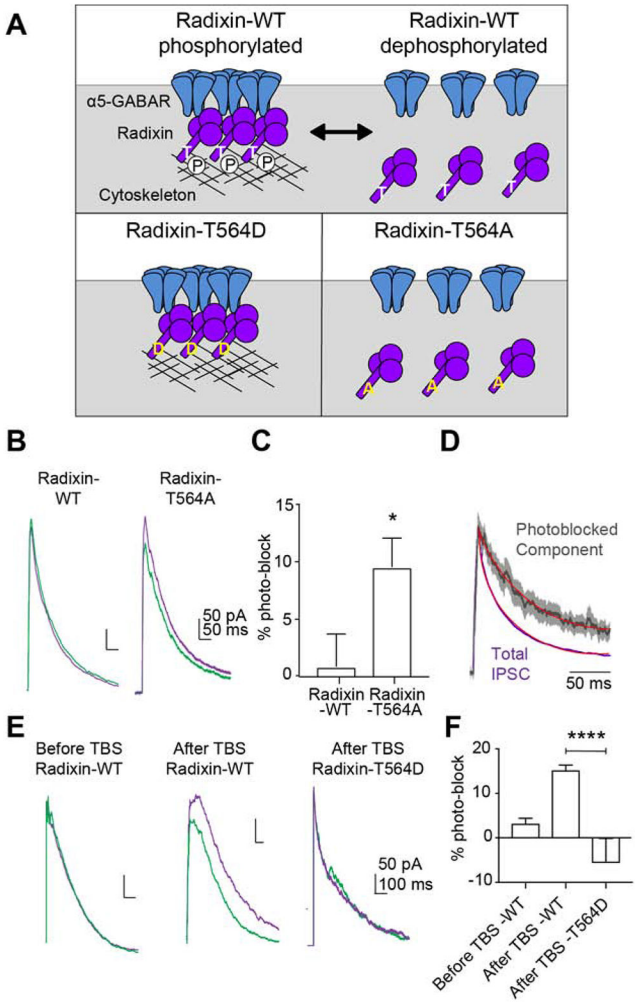

Figure 5. Radixin dephosphorylation mediates TBS-induced synaptic redistribution of α5-GABAR in hippocampal slices.

A. Radixin phosphorylation mutants for manipulating α5-GABAR binding.

B. Photo-block had no effect on IPSCs in WT neurons, but reduced IPSC amplitude in neurons expressing radixin-T564A.

C. Quantification of photo-block of IPSCs in radixin-T564A overexpression shows significant increase in α5-GABAR component compared to control, N = 7-10 cells.

D. Normalized overlaid total IPSCs (black) and the light sensitive component (I_{380}-I_{540}) mediated by α5-GABARs (red). Decay time (red, τ = 67.18 ms) of α5 component (red) is slower than total IPSC (τ = 32.99 ms). Area under the ROC curve is significantly different ($p<0.0001$), N = 6-9 cells.

E. Radixin-T564D prevents TBS-induced redistribution of α5-GABARs to synapses. Photo-block reduced IPSC amplitude after TBS in WT neurons, but not radixin-T564D expressing neurons.

F. Quantification of photo-block of IPSCs in control vs. radixin-T564D overexpression before and after TBS. Radixin-T564D overexpression prevents movement of α5-GABARs compared to control, N = 5-9 cells.

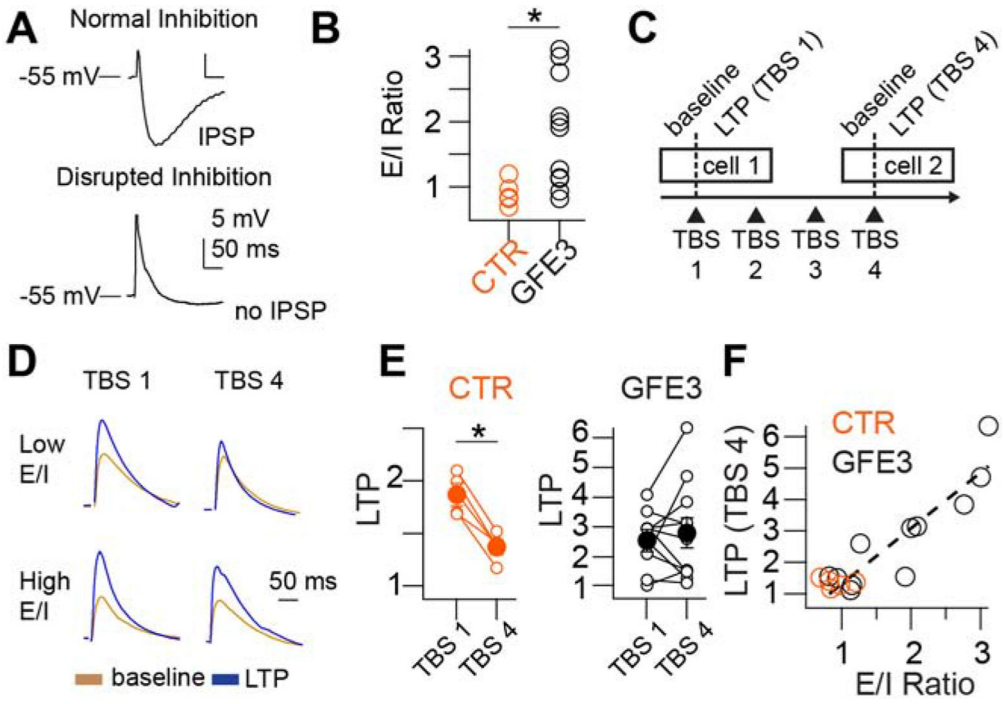

Figure 6. Inhibitory synapses are necessary for activity-dependent α5-GABAR suppression of cumulative LTP.

A. Postsynaptic voltage response in a CA1 neuron depolarized to −55 mV with current injection. Cell with large hyperpolarizing component (10 mV) reflects normal inhibition (low E/I ratio). Cell with small hyperpolarizing component (<1 mV) reflects disrupted inhibition (high E/I ratio).

B. The distribution of E/I ratios from control slices and slices expressing GFE3-GFP. N = 5 control, 11 GFE3 cells.

C. Experimental timeline. Baseline and LTP induced by TBS were recorded in a naive cell (cell 1) and separately in a previously potentiated cell (cell 2). TBS were delivered 20 minutes apart.

D. LTP saturates in cells with low E/I ratio, but not those with high E/I ratio. Postsynaptic voltage responses before (gold traces) and after (blue traces) the first TBS and fourth TBS in cells with either high or low E-I ratios. Traces are normalized to equalize baseline response amplitudes (gold traces).

E. LTP values in control slices (orange), or slices infected with AAV-GFE3-GFP (black). Lines connect 1st TBS and 4th TBS LTP measurements in the same slice. Filled symbols represent mean LTP amplitude. N = 5 control cells, 11 GFE3 cells.

F. Disrupted inhibition is correlated with reduced LTP saturation. LTP induced after the 4th TBS plotted against E/I ratio. Data is from non-transduced slices (orange) and GFE3-transduced slices (black). Dotted line is a linear fit to GFE3 data points.

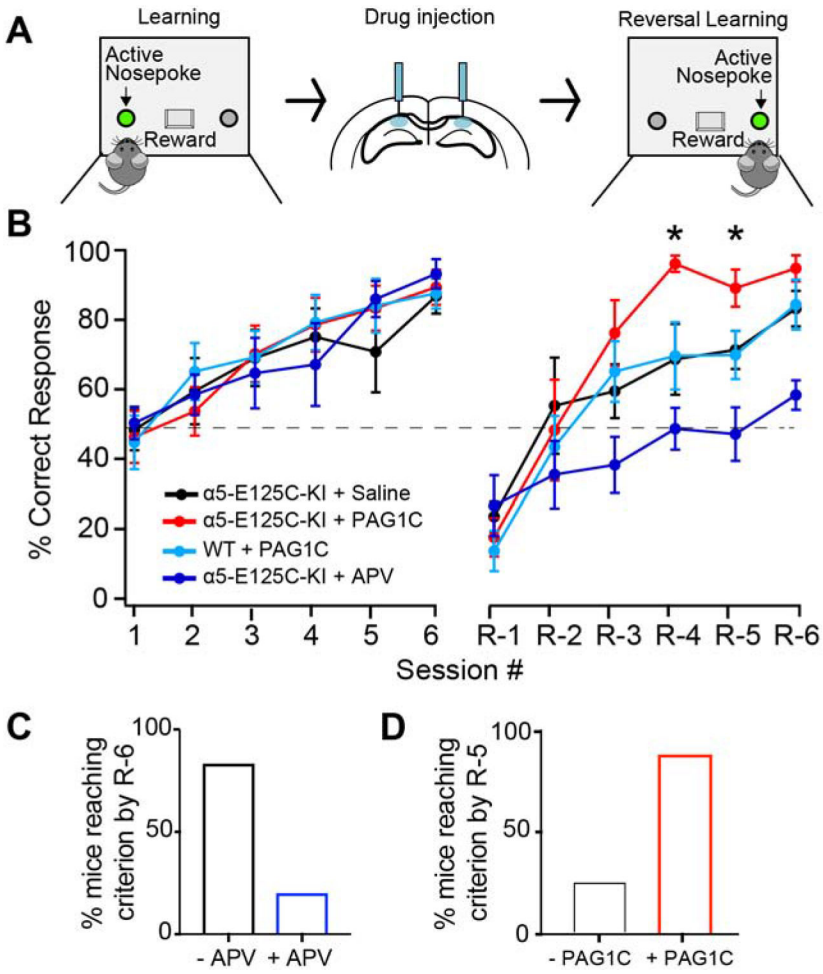

Figure 7: Reversal learning is enhanced by blocking hippocampal α5-GABARs *in vivo*.

A. Schematic of the experimental procedure. Learning was elicited by 2 operant conditioning sessions per day for 3 days. Subsequently, reversal learning was elicited by 6 reversal sessions within 1 day. Session duration was 15 min. PAG1C, APV, or saline were injected 1 hour prior to the start of reversal learning (Figure S8).

B. WT mice injected with PAG1C (light blue, n = 8 mice) and α5-E125C-KI mice injected with saline (black; n = 8 mice) showed the same reversal learning trajectories. However, α5-E125C-KI mice injected with PAG1C (red, n = 8 mice) showed accelerated reversal learning at trial R-4. Injection with APV impaired reversal learning (dark blue, n = 8 mice).

C. Impairment of reversal learning in α5-E125C-KI mice injected with NMDAR blocker APV compared to vehicle. Quantification of reversal learning, defined as the minimal number of trials required to reach criterion (75% correct) after stimulus reversal.

D. Enhancement of reversal learning in α5-E125C-KI mice injected with PAG1C compared to vehicle.

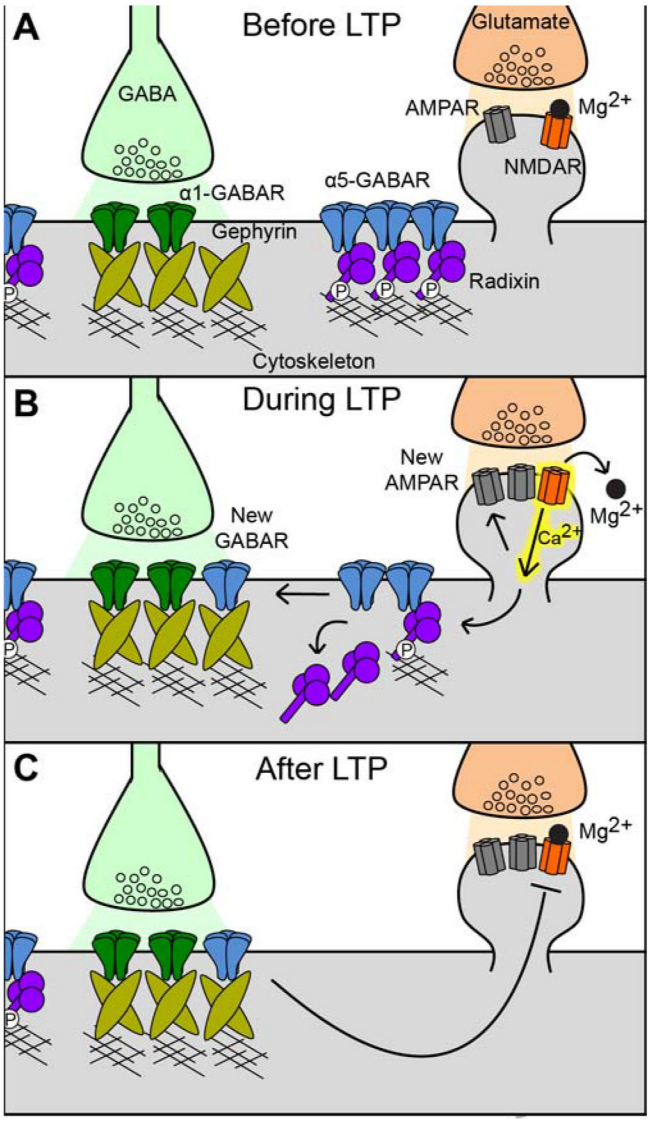

Figure 8. Steps in α5-GABAR suppression of cumulative LTP.

A. At rest, α5-GABARs are bound to phosphorylated radixin, sequestering the receptors extrasynaptically. Low or moderate stimulation of an excitatory input (orange terminal) results in direct AMPAR-mediated EPSPs and indirect α1-GABAR-mediated fast IPSPs from inhibitory interneurons (light green terminal).

B. High frequency stimulation of the excitatory input activates NMDARs, leading to elevated intracellular Ca^{2+}. This leads to induction of excitatory LTP, mediated by insertion of new AMPARs. Intracellular Ca^{2+} also promotes dephosphorylation of radixin, allowing α5-GABARs to dissociate from their extrasynaptic cache, diffuse laterally in the plasma membrane, and become trapped at inhibitory synapses by the gephyrin.

C. Subsequent high frequency stimulation elicits AMPAR-mediated EPSPs, α1-GABAR-mediated fast IPSPs, and a slower component of the IPSPs mediated by α5-GABARs. The

longer-lasting IPSPs suppress voltage-dependent Mg^{2+} unblock of NMDARs, preventing Ca^{2+} influx through NMDARs, thereby preventing induction of more LTP.

Key Resources Table

REAGENT or RESOURCE	SOURCE	IDENTIFIER
Antibodies		
Anti-GABA A Receptor alpha 5 antibody	Abcam	Ab10098
Anti-ß-Actin Antibody	RayBiotech	P60709
Anti-GABA A Receptor alpha 5 antibody	Neuromab	N415/24
Bacterial and Virus Strains		
pAAV-Ef1a-DIO_EGFP-GFE3	Addgene	79871
AAV-flex-ReaChR-citrine	Addgene	50955
AAV9-hSyn-a5(E125C)-eGFP	Lin et al. 2015	n/a
AAV9-Radixin-T654A	This paper	n/a
AAV9-Radixin-T564D	This paper	n/a
Biological Samples		
none		
Chemicals, Peptides, and Recombinant Proteins		
PAG-1C	Lin et al. 2015	n/a
TB-21007	Tocris	2905
Picrotoxin	Tocris	1128
Kynurenic Acid	Hellobio	NB0362
APV	Sigma	A5282
MK-801	Tocris	0924
TCEP	Sigma	646547
DNQX	Tocris	2312
Critical Commercial Assays		
WES	Proteinsimple	n/a
Quikchange mutagenesis kit	Agilent	200519
Deposited Data		
none		

REAGENT or RESOURCE	SOURCE	IDENTIFIER
Experimental Models: Cell Lines		
none		
Experimental Models: Organisms/Strains		
Alpha 1 E125C knock-In mouse	Jackson Laboratory	028965
Alpha 5 E125C knock-in mouse	This paper	n/a
SST-IRES-CRE mouse	Jackson Laboratory	013044
PV-IRES-CRE mouse	Jackson Laboratory	008069
Alpha 5 GABAR knockout mouse	Dr. Uwe Rudolph	n/a
C57BL/6J	Jackson Laboratory	000664
Oligonucleotides		
none		
Recombinant DNA		
none		
Software and Algorithms		
PClamp	Molecular Devices	n/a
Igor	Wavemetrics	n/a
Matlab	Mathworks	n/a
Excel	Microsoft	n/a
Sigmaplot	Systat	n/a
Image J	Image J	n/a
WinLTP	WinLTP Ltd.	n/a
Other		
Spectra-X Light Engine	Lumencor	

REAGENT or RESOURCE	SOURCE	IDENTIFIER